A dual-acting 5-HT 6 receptor inverse agonist/MAO-B inhibitor displays glioprotective and pro-cognitive properties

Vittorio Canale, Katarzyna Grychowska, Rafal Kurczab, Mateusz Ryng, Abdul Raheem Keeri, Abdul Raheem Keeri, Grzegorz Satala, Agnieszka Olejarz-Maciej, Paulina Koczurkiewicz, Marcin Drop, et al.

A dual-acting 5-HT$_6$ receptor inverse agonist/MAO-B inhibitor displays glioprotective and pro-cognitive properties

Vittorio Canale,[a] Katarzyna Grychowska,[a] Rafał Kurczab,[b] Mateusz Ryng,[b] Abdul Raheem Keeri,[a] Grzegorz Satała,[b] Agnieszka Olejarz-Maciej,[c] Paulina Koczurkiewicz,[d] Marcin Drop,[a] Klaudia Blicharz,[a] Kamil Piska,[d] Elżbieta Pękala,[d] Paulina Janiszewska,[e] Martyna Krawczyk,[f] Maria Walczak,[e] Severine Chaumont-Dubel,[g] Andrzej J. Bojarski,[b] Philippe Marin,[g] Piotr Popik,[f] Paweł Zajdel[a],*

[a] *Jagiellonian University Medical College, Department of Medicinal Chemistry,* [c] *Department of Technology and Biotechnology of Drugs,* [d] *Department of Pharmaceutical Biochemistry* and [e] *Department of Toxicology, 9 Medyczna Str., 30-688 Kraków, Poland*
[b] *Maj Institute of Pharmacology, Polish Academy of Sciences, Department of Medicinal Chemistry,* [f] *Department of New Drug Development, 12 Smętna Str., 31-324 Kraków, Poland*
[g] *Institut de Génomique Fonctionelle, Université de Montpellier, CNRS INSERM, 34094 Montpellier, France*

*Corresponding author:
Paweł Zajdel
Department of Medicinal Chemistry
Jagiellonian University Medical College
E-mail: pawel.zajdel@uj.edu.pl
Tel.: +48 126205450

1

Abstract

The complex etiology of Alzheimer's disease has initiated a quest for multi-target ligands to address the multifactorial causes of this neurodegenerative disorder. In this context, we designed dual-acting 5-HT$_6$ receptor (5-HT$_6$R) antagonists/MAO-B inhibitors using pharmacophore hybridization strategy. Our approach involved linking 5-HT$_6$R scaffolds with aryloxy fragments derived from reversible and irreversible MAO-B inhibitors. The study identified compound **48** that acts as an inverse agonist of 5-HT$_6$R at G$_s$ signaling and an irreversible MAO-B inhibitor. Compound **48** showed moderate metabolic stability in rat microsomal assay and artificial membrane permeability, and it was well distributed to the brain. Additionally, **48** showed glioprotective properties in a model of cultured astrocytes using 6-OHDA as the cytotoxic agent. Finally, compound **48** (MED = 1 mg/kg, *p.o.*) fully reversed memory deficits in the NOR task induced by scopolamine in rats. A better understanding of effects exerted by dual-acting 5-HT$_6$R/MAO-B modulators may impact the future development of neurodegenerative-directed treatment strategies.

1. Introduction

Neurodegenerative diseases are chronic conditions which involve progressive loss of neuronal and glial cells, demyelination, and overall structural and functional brain deficits. Among these diseases, Alzheimer's disease (AD) is the most common disorder characterized by continuous deterioration of cognitive functions, resulting in complete disability in the elderly life. The increasing prevalence of AD, together with the lack of effective therapy that could slow down the progression of the disease, makes it one of the biggest global health challenge0

Unfortunately, therapeutically useful disease-modifying and symptomatic drug candidates for AD developed in the two past decades have shown disappointing results.[1–3] Nonetheless, our understanding of G protein-coupled receptors (GPCRs) signaling networks, and compensatory mechanisms related to enzyme inhibition[4] and disease pathology steadily grew, thereby opening new opportunities for drug discovery. In particular, more focus was given to develop new strategies using multi-target directed ligands (MTDL) to address the etiology and symptoms of such a complex and debilitating disease. Accumulating evidence revealed that connecting and/or merging structural fragments, which simultaneously affect different biological targets, is one of the most promising areas of anti-AD drug development.[5,6] Several MTDLs have been reported, with the most prominent examples being dual enzymatic inhibition of acetylcholinesterase (AChE) and glycogen synthase kinase (GSK-3β),[7] inhibition of AChE and monoamine oxidase B (0)[8] and inhibition of β-secretase (BACE-1) and GSK-3β.[9] The MTDL strategy is further completed with GPCRs dual-acting compounds as 5-HT$_6$/D$_3$ and 5-HT$_{2A}$/5-HT$_6$ receptor antagonists[10–13] as well as 5-HT$_4$R agonist/5-HT$_6$R antagonist.[14] However, simultaneous targeting of enzyme and receptor activities constitutes a more challenging area. This stems from limitations in finding common binding modes and structural features for targets with different location and structural requirements.[15] Among examples of such an approach, the dual-acting compounds described thus far include AchE inhibitors and NMDA receptor antagonists,[16] AChE and histamine H$_3$ receptor (H$_3$R) antagonists,[17] AChE inhibitors and sigma σ$_1$ receptor ligands,[18] AChE inhibitors and serotonin 5-HT$_4$R agonists[19] or AChE inhibitors and 5-HT$_6$R antagonists.[20]

Serotonin type 6 receptor (5-HT$_6$R) is a GPCR which has emerged as a promising target for the treatment of pro-cognitive deficits of neurodegenerative and psychiatric disorders. It is almost exclusively expressed in the central nervous system (CNS), particularly in brain regions involved in cognitive processes, i.e., prefrontal cortex, hippocampus and striatum. 5-HT$_6$R is

primarily located in the cilia of neurons which are sensory organelles that participate in neurodevelopment and neuronal differentiation.[21–24]

Pharmacological blockade of 5-HT$_6$R, located on GABA-ergic and glutamatergic neurons, increases cholinergic transmission.[25,26] Consequently, 5-HT$_6$R antagonists show beneficial effects on cognition, as shown by a various preclinical studies and preliminary clinical studies[27–29] that revealed pro-cognitive effects in humans.[30] However, phase III clinical trials for these compounds showed disappointing results.

The recent findings on the elevated level of MAO-B in AD brains, corroborated by data showing a MAO-B-dependent control of amyloid-β production in neurons *via* γ-secretase, suggest a role of MAO-B in AD.[31] MAO-B is mainly found in the outer membrane of the mitochondria in non-neuronal cells, such as glial cells00000 It is a membrane-bound FAD-containing enzyme, involved in the degradation of monoamines, including dopamine. It has been demonstrated that the production of reactive oxygen species, resulting from the activity of MAO-B, increases with age. Furthermore, an elevated level of this enzyme has been found in astrocytes and pyramidal neurons of AD brains.[31,33] Based on these observations, MAO-B inhibitors have been investigated as potential neuroprotective agents for the treatment of neurodegenerative disorders.[34]
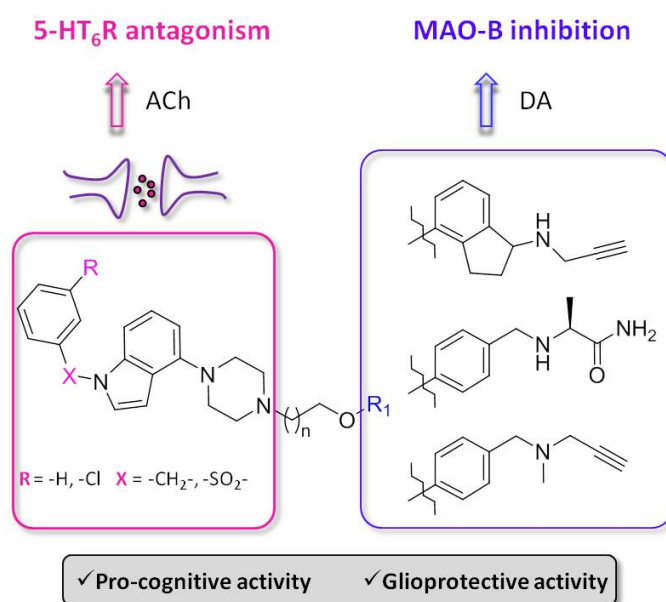

Figure 1. The design strategy of dual-acting 5-HT$_6$R/MAO-B modulators.

To determine how to target two distinct proteins with different pharmacophore requirements, we analyzed the binding mode in the 5-HT$_6$R homology model and sought opportunities to

target MAO-B catalytic center using induced fit-docking (IFD) and quantum mechanics/molecular mechanics (QM/MM) calculations. This prospective *in silico* analysis, guided the design and synthesize a new series of hybrid compounds obtained by linking pharmacophore fragments of 5-HT$_6$R antagonists with molecular frameworks of known MAO-B inhibitors in a unique molecular entity (Fig. 1). Structural modifications comprised functionalization of *N*1 atom of (indol-4-yl)piperazine with 3-chlorobenzyl and benzenesulfonyl moieties in the 5-HT$_6$R substructure and diversification of aryloxy fragments derived from reversible and irreversible MAO-B inhibitors, both connected *via* an alkylene spacer of different length. The alaninamide and propargyl moieties were chosen as the moieties able to interact this FAD fragment in the enzymatic cleft of MAO-B. Here, we evaluated the structure-activity relationship (SAR) within novel dual-acting compounds exhibiting inhibitory activity for 5-HT$_6$R and MAO-B. We selected a lead compound (compound **48**), for which we performed more detailed mechanistic studies. We assessed its action on both targets and examined its distribution to the CNS following peripheral administration. Finally, we showed that this dual 5-HT$_6$R inverse agonist/MAO-B inhibitor protects astrocytes against 6-hydroxydopamine (6-OHDA)-induced toxicity and reverses scopolamine-induced cognitive impairment in the novel object recognition (NOR) task in rats.

2. Chemistry

The designed compounds were synthesized in two stages. First, the respective building blocks, namely functionalized (indol-4-yl)piperazine **5** and **6** (Scheme 1A) and alkylating agents **9–17** (Scheme 1B), were obtained using parallel synthetic routes. Commercially available 4-bromoindole **1** was subjected to Buchwald-Hartwig *N*-arylation to yield 4-(4-Boc-piperazin-1-yl)indole. Simple heating of the obtained product in ethanol at 150 °C using microwave irradiation eliminated Boc protecting function and provided 1*H*-indole intermediate **2**. This was subsequently reacted with 3-chlorobenzyl bromide or benzenesulfonyl chloride, in the presence of phosphazene base (BTPP) to afford indoles **3** and **4**. Treatment of the latter compounds with TFA furnished secondary amines **5** and **6**, respectively.
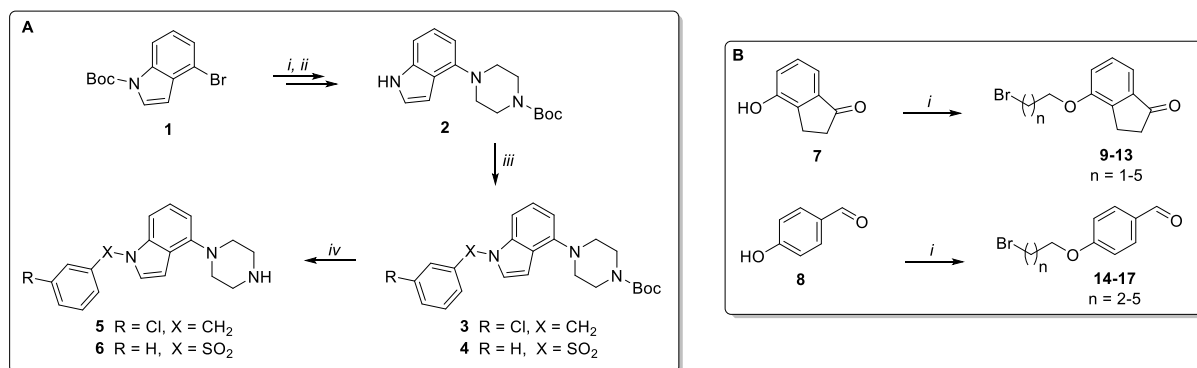
Scheme 1. **A:** synthesis of 4-piperazine-indole cores **5** and **6**. Reagents and conditions: *i*) Boc-piperazine, Pd$_2$(dba)$_3$, BINAP, *t*-BuONa, toluen, 110 °C, 5 h; *ii*) EtOH, 150 °C, MW, 2 h; *iii*) 3-chlorobenzyl bromide or benzylsulfonyl chloride, BTPP, DCM, 0 °C→rt, 2 h; *iv*) TFA/DCM, 2/8 *v/v*, rt, 1 h; **B:** synthesis of alkylating agents **9–17**; *i*) α,ω-dibromoalkane, K$_2$CO$_3$, KOH, KI, acetone, 60 °C, 16 h.

In parallel, commercially available phenols **7** and **8** were reacted with an excess of different α,ω-dibromoalkane in biphasic conditions, to give respective alkylating agents **9–17** (Scheme 2). Intermediates **9–17** were subsequently combined with secondary amines **5** and **6**, yielding derivatives **18–30,** by stirring in acetone at 60 °C, in the biphasic system, for 16 h.

Final compounds **31–48** were obtained by reductive amination, using sodium triacetoxyborohydride (STAB) in THF for primary amines or STAB in DCM for secondary amines.
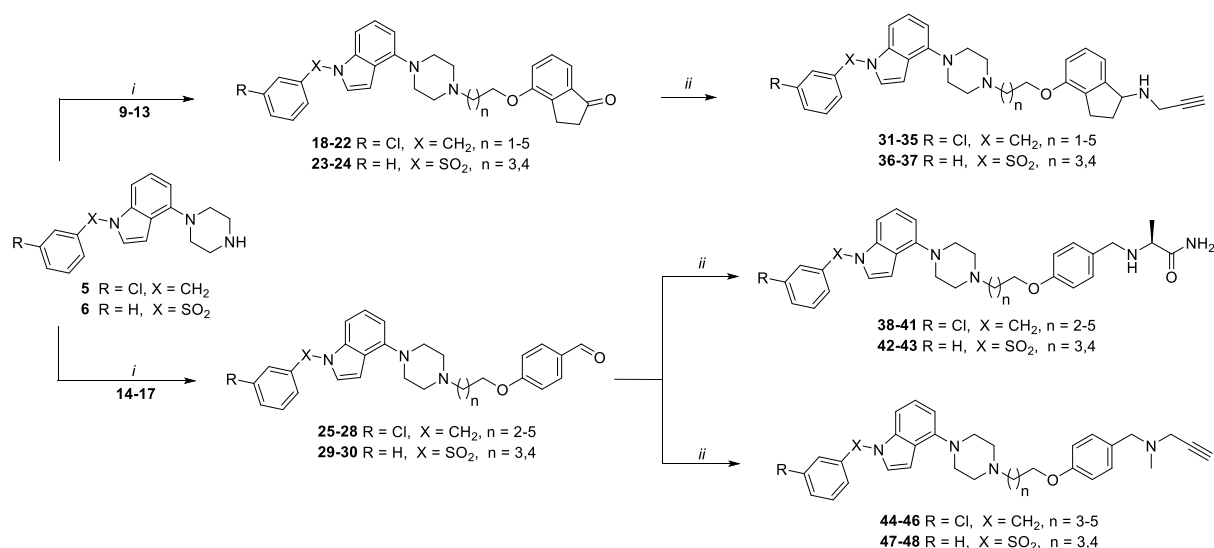
Scheme 2. Synthesis of final compounds **31–48**. Reagents and conditions: *i*) alkylating agent **9–13** or **14–17**, K$_2$CO$_3$, KI, acetone, 60 °C, 16 h; *ii*) for primary amine: AcOH, THF$_{anh}$, rt, 5 h then STAB, rt, 2 h; for secondary amine, AcOH, DCM$_{anh}$, 0.5 h then STAB, rt, 2 h.
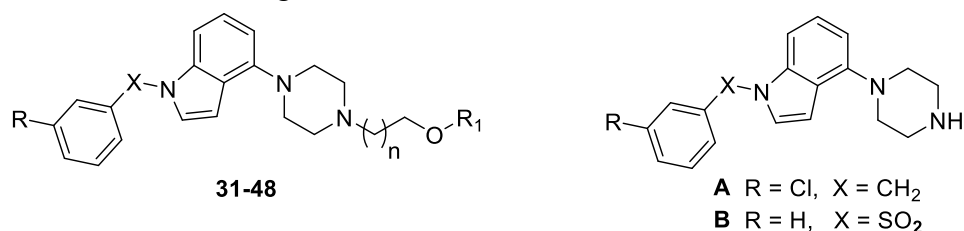
3. Results and discussion

3.1. Structure-activity relationship studies

The molecular framework of the dual-acting derivatives was based on the pharmacophore hybridization strategy supported with prospective *in silico* analysis of homology model of 5-HT_6R and crystal structure of MAO-B. The strategy involved connecting pharmacophore structures of known selective 5-HT_6R antagonists and MAO-B inhibitors in a single molecule. The selection of phenylsulfonyl-4-(piperazin-1-yl)-1*H*-indole (**A**) and *N*-3-chlorobenzyl-4-(piperazin-1-yl)indole (**B**) as 5-HT_6R-targeting fragments, was based on literature and unpublished data. Our data indicated that compounds containing unsubstituted phenylsulfonyl moiety are highly potent 5-HT_6R ligands, whereas their benzyl analogs require substitution with a chlorine atom in the *meta* position.[35]

To achieve inhibition of MAO-B activity, aryloxy fragments derived from rasagiline, safinamide and pargyline were linked to the 5-HT_6R pharmacophore *via* different length alkylene linker. Although the molecular framework of the designed hybrids is different from that of classical MAO-B inhibitors (they are very long, with two basic centers and a flexible alkylene linker), the possibility of interaction with the catalytic domain of MAO-B was supported by *in silico* experiments. Indeed, molecular dynamics studies indicated the existence of two entrance channels to the MAO-B binding site for inhibitors (more details in SI), i.e., membrane accessed (A), and solvent accessed (B).[36] An analysis of ligand-enzyme complexes for MAO-B crystals showed that entrance A is closed for several compounds, whereas entrance B forms a narrow channel. IFD for the designed compounds provided a static view of the conformation of the enzyme, showing that the only way to enter the catalytic center is through entrance B, which is devoid of significant steric hindrances. It should be emphasized here that such large compounds would be unable to enter the catalytic MAO-B through entrance A, because it would be sterically disturbed by the mitochondrial membrane.

The newly synthesized compounds **31–48** showed moderate affinity for 5-HT_6R in ^{3}[H]-LSD binding experiments and low-to-high inhibitory potency for MAO-B, with IC_{50} values ranging from 30 to >1000 nM as assessed using the fluorimetric method (Table 1).

Table 1. Affinity for 5-HT$_6$R and potency for MAO-B inhibition of synthesized compounds **31–48** and reference 5-HT$_6$R ligands and MAO-B inhibitors.

31-48

A R = Cl, X = CH$_2$
B R = H, X = SO$_2$

Compd	R	X	n	R$_1$	K_i [nM][a] h5-HT$_6$R	IC$_{50}$ [nM][b] and (%inh)[c] hMAO-B
31			1		100	> 1000 (35)
32			2		77	> 1000 (31)
33	Cl	CH$_2$	3		113	270 ± 43 (100)
34			4		223	460 ± 51 (80)
35			5		259	> 1000 (34)
36	H	SO$_2$	3		50	> 1000 (44)
37			4		51	163 ± 25 (90)
38			2		158	> 1000 (47)
39	Cl	CH$_2$	3		162	> 1000 (24)
40			4		232	> 1000 (43)
41			5		340	> 1000 (23)
42	H	SO$_2$	3		68	> 1000 (20)
43			4		65	> 1000 (17)
44			3		195	323 ± 42 (85)
45	Cl	CH$_2$	4		140	30 ± 2 (100)
46			5		137	> 1000 (32)
47	H	SO$_2$	3		54	> 1000 (51)
48			4		38	154 ± 19 (91)
A	Cl	CH$_2$			7	(3)
B	H	SO$_2$			0.3	(3)
Intepirdine[d]					1.4	-
Rasagiline					-	15.4 ± 0.6 (100)
Safinamide					-	7 ± 1.2 (100)

[a]Mean K_i values (SEM ± 15%) based on three independent binding experiments

[b] IC$_{50}$ ± SEMs values were determined using rasagiline [1 μM] as positive control

[c] % of inhibition of control (rasagiline, 1 μM) at 1 μM

[d] Data taken from [28]

Generally, linking 5-HT$_6$R pharmacophores with MAO-B-targeting fragments decreased affinity for 5-HT$_6$R when compared with the parent compounds **A** and **B**. However, this modification did not totally preclude the interaction of the obtained derivatives with the binding

cavity of 5-HT$_6$R (K_i = 38–340 nM). Compounds bearing N1-sulfonyl moiety were more potent 5-HT$_6$R ligands than their congeners with methylene bridge, regardless of the length of the alkylene linker and the kind of MAO-B fragment (**34** *vs* **37** and **44** *vs* **47**). Analysis of the obtained ligand-receptor complexes for compound **48** exhibiting the highest affinity for 5-HT$_6$R (Fig. 2A), showed that the protonated piperazine fragment formed a salt bridge with D3.32, the indole ring was positioned in the conserved aromatic cluster of F6.51 and F6.52, and the terminal phenyl ring was accommodated in a hydrophobic cavity formed by transmembrane domains 3–5 and extracellular loop 2. It should be noted that the indole and phenyl rings form an angle of approximately 90°, resulting from the tetrahedral geometry (sp^3) of sulfonyl linkers. In turn, the propargyl moiety at the aryloxy fragment was directed toward the extracellular part of the receptor, with the phenyl ring positioned between N2.63 and W7.39, and protonated the N-methyl-propargylamine forming a salt bridge with D7.35.
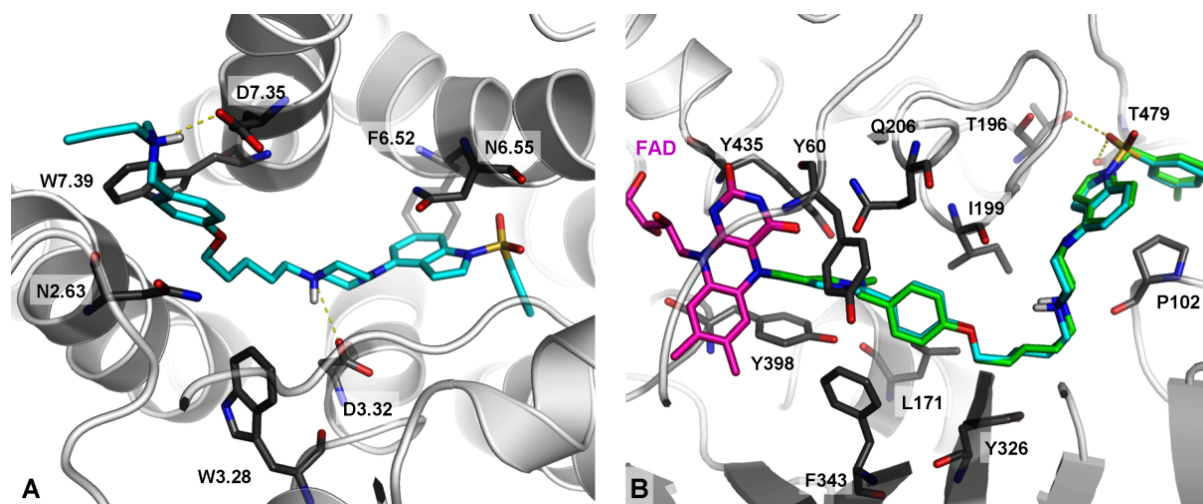

Figure 2. The binding mode of **48** (cyan) in 5-HT$_6$R (A), and comparison of binding modes of **45** (green) and **48** (cyan) in the MAO-B catalytic site (B).

Exploration of SAR toward MAO-B revealed that sulfonamide derivatives were less preferred for the interaction with the enzymatic target than their benzyl analogs (**33** *vs* **36, 40** *vs* **43**, and **44** *vs* **47**). With regard to the length of the alkylene chain, four and five methylene linked hybrids (**40**, **33**) exhibited the highest inhibition activity ranging from 73% to 100% in all evaluated series. More detailed analysis of the aryloxy terminal fragment, indicated that compounds **38–43** bearing safinamide-derived alaninamide moiety, showed low inhibitory potency against enzyme. On the other hand, the presence of propargyl- and N-methyl-propargylamine (originated from rasagiline and pargyline, respectively) increased the inhibitory effect (31–100% inhibition), thus highlighting the pivotal role of covalent bond

formation of compounds **33**, **37**, **45** and **48** with FAD cofactor in the enzymatic target. This observation was further confirmed by *in silico* studies. The binding modes of the most potent MAO-B inhibitors **45** and **48** (Fig. 2B) were coherent and showed accommodation of the molecules in an "aromatic cage" formed by Y435, Y398, Y60, and F343, which are considered crucial in the ligand positioning for the reaction with FAD.[37–39] Additionally, the hydrogen bond between the side chain of Q206 and the nitrogen atom of the propargyl functional group seems to play a role in placing this fragment in an optimal position.[39]

3.2. Determination of selectivity profile for compound 48

The SAR analysis allowed to identify the most potent dual-acting compound **48** possessing a phenylsulfonyl moiety at (indol-4-yl)piperazine scaffold in tandem with aryloxy fragments derived from pargyline, connected *via* a four methylene spacer (K_i 5-HT$_6$R = 38 nM, IC$_{50}$ MAO-B = 154 nM). Subsequently, compound **48** was profiled *in vitro* for selectivity over structurally-related GPCRs and MAO-A enzyme isoform (Table 2).

Table 2. Binding data of selected compound **48** and intepirdine for 5-HT$_6$, 5-HT$_{1A}$, 5-HT$_{2A}$, 5-HT$_7$, and D$_2$Rs and IC$_{50}$ values for MAO-B and inhibitory activity at MAO-A.

Compd	K_i [nM][a]					IC$_{50}$[b]	
	5-HT$_6$	5-HT$_{1A}$	5-HT$_{2A}$	5-HT$_7$	D$_2$	MAO-B	MAO-A
48	38	684	420	7996	813	154	1037
Intepirdine[c]	1.4	2370	26	14230	997	NT[d]	NT[d]

[a] Mean K_i values (SEM ± 25%) based on three independent binding experiments
[b] IC$_{50}$ ± SEMs values was determined using rasagiline [1 µM] or clorgyline [1 µM] as positive control for MAO-B and MAO-A, respectively
[c] data taken from [28]
[d] Not Tested

Compound **48** showed moderate to high selectivity over 5-HT$_{1A}$, 5-HT$_{2A}$, 5-HT$_7$, and D$_2$ receptors. Although it contains aryloxy fragments derived from pargyline (a known non-selective MAO inhibitor), it showed moderate inhibitory activity toward the MAO-A enzyme isoform, thus reducing the possibility to elicit cardiovascular side effects (i.e., hypertensive crisis).

To exclude potential risks related to undesired cardiovascular or CNS side effects, the affinity of compound **48** for selected "off-target" receptors was assessed by Eurofins Scientific. The tested compound displayed low affinity for α$_{1A}$ adrenoreceptor (% inhibition at 1

μM = 37%) and did not bind to β_1 adrenoreceptor (% inhibition at 1 μM = 5%), H_1 histaminic receptor (% inhibition at 1 μM = 13%) and M_1 muscarinic receptor (% inhibition at 1 μM = 4%).

3.3. Impact of compound 48 on 5-HT₆R-operated signaling and on MAO-B activity

The impact of compound **48** on adenylate cyclase activity was first examined in 1321N1 cells expressing 5-HT₆R and treated with 5-Carboxamidotryptamine (5-CT), a 5-HT₆R agonist. Compound **48** behaved as a potent antagonist of 5-HT₆R in this cellular assay (K_b = 6 nM, Table 3).

Table 3. The antagonist property of compound **48** and intepirdine in 1321N1 cells and their functional activity at 5-HT₆R-dependent Gs signaling in NG108-15-based model.

Compd	K_b [nM][a]	IC_{50} [nM][b]	Functional profile
		5-HT₆	
48	6± 1	860 ± 0.68	Inverse Agonist
Intepirdine	1.3± 0.2	97 ± 0.21	Inverse Agonist

[a] Mean K_b ± SEMs of values obtained in three independent experiments in 1321N1 cells
[b] Mean IC_{50} ± SEMs of values obtained in three independent experiments in NG108-15 cells

The high level of constitutive activity of 5-HT₆R, defined as the ability of the receptor to adopt an active conformation able to transduce signal in the absence of an agonist, has been demonstrated in both *in vitro* and *ex vivo* models.[40,41] This property opens up the possibility to classify 5-HT₆R ligands as inverse agonists or neutral antagonists.[28,42]

Hence, the ability of compound **48** to modulate agonist-independent 5-HT₆R-operated Gs signaling was tested in NG108-15 cells transiently expressing 5-HT₆R, a cellular model in which the receptor displays high constitutive activity.[41,43] We found that compound **48** decreased basal cAMP level in a concentration-dependent manner (IC_{50} = 860 ± 0.68 nM) but its apparent affinity was much lower than that of the prototypic 5-HT₆R inverse agonist intepirdine (Table 3, Fig. 3).
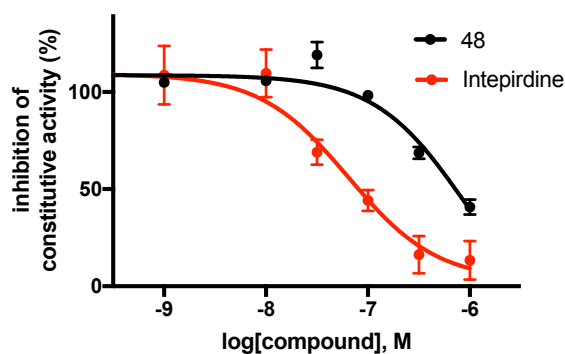
Figure 3. Influence of compound **48** and intepirdine on basal cAMP production in NG108-15 cells transiently expressing 5-HT$_6$Rs. Data are the means ± SEM of the values obtained in three independent experiments performed in quadruplicate in different sets of cultured cells. ***p < 0.001 *vs.* vehicle (ANOVA followed by Student−Newman−Keuls test).

To investigate the inhibitory mechanism of compound **48** on *h*MAO-B, time-dependent inhibition studies were performed using *in vitro* method. Rasagiline and safinamide, with known irreversible and reversible inhibition toward MAO-B were used as reference drugs (Fig.4). In the case of reversible inhibitor safinamide, the competing excess of p-tyramine, used as an enzyme substrate, significantly reactivated the enzyme activity. In contrast, rasagiline, depending on the pre-incubation time used, has either slightly restored MAO-B activity or maintained only residual activity of the enzyme. A higher than expected signal for rasagiline without pre-incubation (ca. 30% reactivation) might be explained by the longer time required to create the covalently bound inhibitor-enzyme complex by irreversible inhibitors. Although compound **48** was able to restore some activity of MAO-B, the difference between the enzyme reactivation rate, obtained with and without pre-incubation, suggests that compound **48** covalently modify the enzyme.
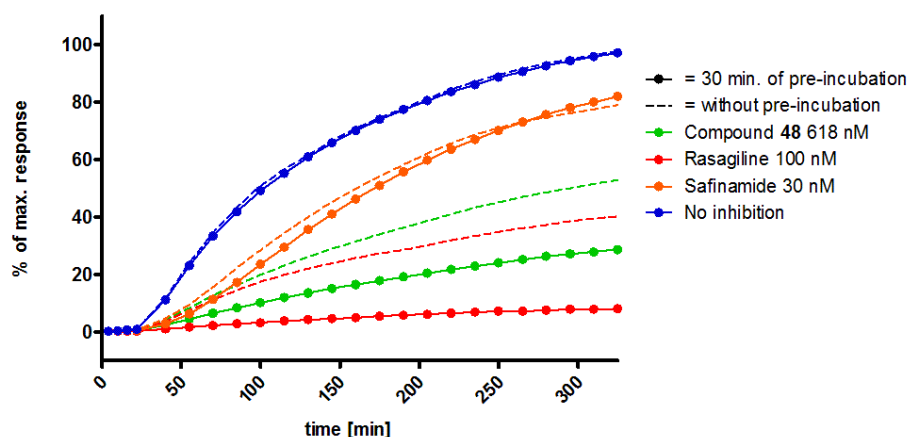

Figure 4. Reactivation of MAO-B activity upon blockade with compound **48** and reference inhibitors used at a concentrations corresponding to their IC$_{80}$ values in the presence of the

substrate p-tyramine. All compounds were tested with 30 min of pre-incubation (rings) and without pre-incubation (lines). Data are presented as mean values from two independent experiments run in duplicate. The results were normalized to the effect induced by 1 mM of p-tyramine (100 % value) and solvent (0 % value) in the last measurement of the experiment.

3.4. Preliminary evaluation of ADME properties

As ligands that combine two pharmacophore fragments within a single molecule usually have physicochemical properties burdens (high molecular weight or clog P value), which might limit their bioavailability, compound **48** was subsequently evaluated for its drug-likeness in *in vitro* screening. The ability to cross the blood-brain barrier (BBB) by passive diffusion was assessed by the commonly used parallel artificial membrane permeability assay (PAMPA-BBB).[44] Compound **48** showed an efficient permeability (Pe) value greater than 4.0 in the tested conditions, thus suggesting a high CNS penetration (Table 4). The reference drugs verapamil (Pe = 1.85×10^{-5} cm/sec) and doxorubicin (not detected in the acceptor compartment) were used as positive and negative control, respectively.

Table 4. Summary of the ADME profile evaluation for compound **48**

Assay type	48
PAMPA permeability	Pe = 4.84×10^{-6} cm/sec[a]
Microsomal stability	Cl_{int} = 85 ml/min/kg[b]
Preliminary *in vivo* pharmacokinetics[c]	C_{max} = 72.7 ng/mL T_{max} = 30 min

[a] measured at 100 μM initial concentration at pH 7.4 in a phosphate buffer at room temperature measured at pH 7.4 in a phosphate buffer at room temperature
[b] determined at a protein concentration of 0.4 mg/ml in RLM assay
[c] measured after *p.o.* administration of dose 3 mg/kg.

Subsequently, the *in vitro* metabolic stability of compound **48** was determined using rat liver microsomes (RLMs). After 60-min incubation period, the compound **48** showed an average intrinsic clearance (Cl_{int}) of 85 mL/min/kg (Table 4).

Next, the preliminary pharmacokinetic profile of compound **48** was estimated in male Wistar rats injected with a single dose (3 mg/kg *p.o.*). Compound **48** was rapidly absorbed and was able to cross the BBB with a C_{max} value reaching 72.7 ng/mL in the brain after 30 min (T_{max}, Table 4). The molecule was eliminated very slowly from the rat body, with along half-life of ca. 28 h.

3.5. Glioprotective effects

Given the supporting role of glial cells in the CNS, protection of astrocytes might be a relevant strategy for treating neurodegenerative disorders in addition to directly act on neuronal cell functions or survival [ref]. We thus explored the glioprotective effects of compound **48** in a model of cultured astrocytes (C8-D1A astrocytes) exposed to the neurotoxin 6-OHDA. 6-OHDA-induced cell death is attributed to the oxidative damage by reactive oxygen species (ROS) derived from 6-OHDA autooxidation or possible direct effect of 6-OHDA on the mitochondrial respiratory chain complex.

As revealed by the MTT assay (which assesses mitochondrial metabolism), compound **48** did not induce significant toxicity in C8-D1A astrocyte cultures at concentrations up to 50-100 μM but protected C8-D1A astrocytes against 6-OHDA-induced cytotoxicity (Fig. 5A). These observations were confirmed in lactate dehydrogenase (LDH) assay, which assesses cell membrane integrity (Fig. 5B). Notably, intepirdine exhibited no glioprotective properties.[11] Similarly, although neuroprotective activity of selegiline was established in several *in vitro* models[45–47], this irreversible MAO-B inhibitor did not reduce gliotoxicity induced by 6-OHDA in both cell-based assays (Fig. 5A and 5B). These findings suggest that blockade of MAO-B alone is not sufficient to protect C80D1A astrocytes against 6-OHDA toxicity, and that the glioprotective effect of compound **48** results either from 5-HT$_6$ receptor antagonist/inverse agonist activity or from its dual inhibitory activities on 5-HT$_6$R and MAO-B.
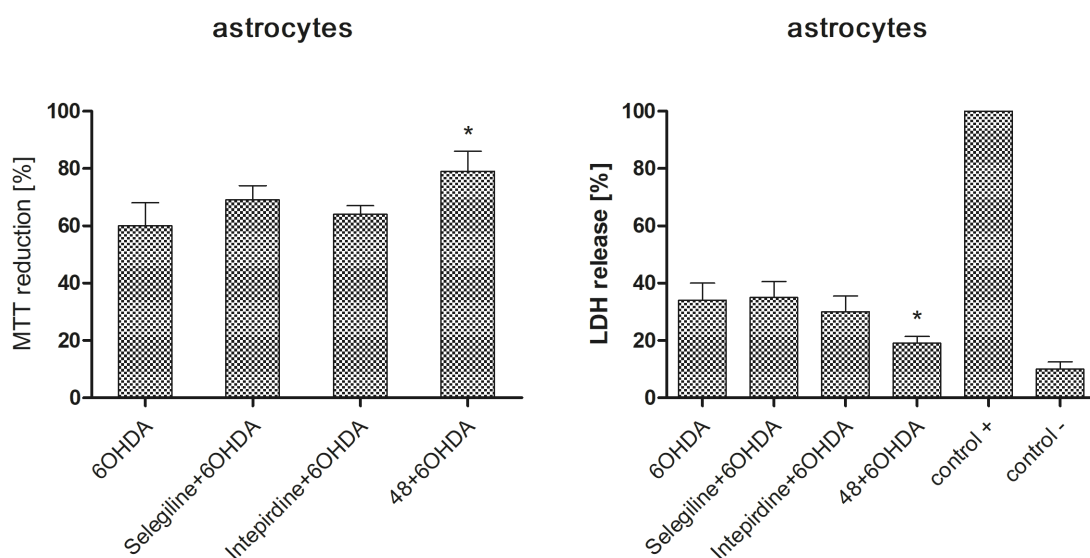

Figure 5. Effect of selegiline, intepirdine, and **48** on 6-OHDA-induced astrocytes cytotoxicity. (A) MTT and (B) LDH assays were performed on astrocytes pre-treated with the tested

compounds (0.25 μM) for 24 h and injured by 6-OHDA (25 μM) for the next 24-h period. p<0.05 *vs* 6-OHDA.

3.6. Pro-cognitive properties

Given the interesting multipotent activity of compound **48**, its ability to rescue cognitive deficit induced by scopolamine (SCOP) in rats was then investigated using the NOR test. Scopolamine administration (1.25 mg/kg, *p.o.*) abolished the ability of rats to discriminate between novel and familiar objects when compared to the vehicle-treated animals. These deficits were significantly reversed by *p.o.* administration of compound **48** at the doses of 1 and 3 mg/kg (Fig. 6).
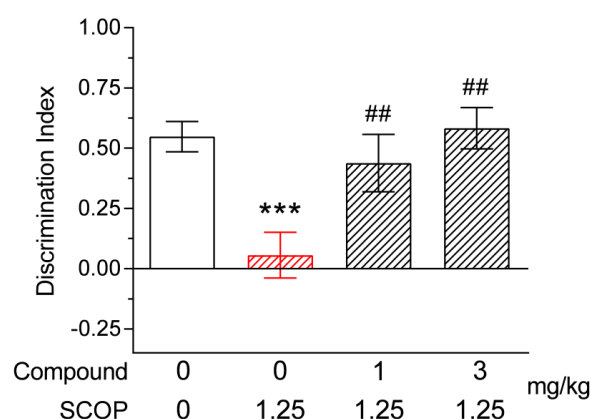

Figure 6. Effects of compound **48** on SCOP-induced inhibition of novelty discrimination in the NOR test in rats. The data illustrated represent discrimination index (DI) and are the mean ± standard error of the mean of N = 6-10 animals per group. Symbols: *** $p < 0.001$ *vs* vehicle-treated group; ## $p < 0.01$ *vs* SCOP-treated group.

Conclusions

Using the strategy of dual-acting compounds, we designed and synthesized a series of hybrids that combine a (indol-4-yl)-piperazine fragment—a well-established core of 5-HT$_6$R antagonists—with frameworks of known MAO-B inhibitors, connected through an alkylene linker. In agreement with the design rationale, the majority of novel hybrid compounds showed affinity for 5-HT$_6$R and inhibitory activity for the enzyme target. The study identified compound **48**, a dual 5-HT$_6$R/MAO-B modulator, which behaved as an inverse agonist of 5-HT$_6$R at the G$_s$ signaling pathway and an irreversible MAO-B inhibitor. Besides showing the most efficient combination of 5-HT$_6$R modulation and MAO-B inhibitory activity, compound **48** was metabolically stable and brain penetrant. Moreover, compound **48** reduced the gliotoxic effect of 6-OHDA in C8-D1A astrocytes in two complementary assays (MTT and LDH)

assessing cell survival. Importantly, this effect was not observed after treatment with intepirdine (5-HT$_6$R antagonist) and MAO-B inhibitor selegiline. Finally, compound **48** also reverse cognitive decline induced by scopolamine in the NOR test. These properties highlight **48** as an original example of dual 5-HT$_6$R/MAO-B modulator and as an interesting prototype in the development of new treatment strategies for AD.

4. Experimental procedures

4.1. Chemistry
4.1.1. General methods

The synthesis was carried out at ambient temperature, unless indicated otherwise. Organic solvents (from Aldrich and Chempur) were of reagent grade and were used without purification. All reagents (Sigma-Aldrich, Fluorochem, Across and TCI) were of the highest purity. Column chromatography was performed using silica gel Merck 60 (70–230 mesh ASTM).

Mass spectra were recorded on a UPLC-MS/MS system consisted of a Waters ACQUITY® UPLC® (Waters Corporation, Milford, MA, USA) coupled to a Waters TQD mass spectrometer (electrospray ionization mode ESI-tandem quadrupole). Chromatographic separations were carried out using the Acquity UPLC BEH (bridged ethyl hybrid) C18 column; 2.1 × 100 mm, and 1.7 μm particle size, equipped with Acquity UPLC BEH C18 Van Guard pre-column; 2.1 × 5 mm, and 1.7 μm particle size. The column was maintained at 40°C, and eluted under gradient conditions from 95% to 0% of eluent A over 10 min, at a flow rate of 0.3 mL min^{-1}. Eluent A: water/formic acid (0.1%, v/v); eluent B: acetonitrile/formic acid (0.1%, v/v). Chromatograms were made using Waters eλ PDA detector. Spectra were analyzed in 200–700 nm range with 1.2 nm resolution and sampling rate 20 points/s. MS detection settings of Waters TQD mass spectrometer were as follows: source temperature 150 °C, desolvation temperature 350°C, desolvation gas flow rate 600 L h-1, cone gas flow 100 L h-1, capillary potential 3.00 kV, cone potential 40 V. Nitrogen was used for both nebulizing and drying gas. The data were obtained in a scan mode ranging from 50 to 2000 m/z in time 1.0 s intervals. Data acquisition software was MassLynx V 4.1 (Waters). The UPLC/MS purity of all the final compounds was confirmed to be 95% or higher.

^{1}H NMR and ^{13}C NMR spectra were obtained JOEL JNM-ECZR500 RS1 (ECZR version) at 500 and 126 MHz, respectively and are reported in ppm using deuterated solvent for calibration (CDCl$_3$ or DMSO-d_6). The J values are reported in Hertz (Hz), and the splitting patterns are designated as follows: br. s. (broad singlet), s (singlet), d (doublet), t (triplet), q (quartet), dd (doublet of doublets), m (multiplet).

Elemental analysis for C, H, N and S was carried out using the elemental Vario EI III Elemental Analyser (Hanau, Germany). All values are given as percentages, and were within ±0.4% of the calculated values.

Compound **48** selected for behavioral evaluation was converted into the hydrochloride salt.

All synthetic procedures and spectroscopic data for selected final compounds are summarized below, while characterization data for all intermediates and remained final compounds are reported in the Supporting Information.

4.1.2. General procedure for the N-arylation of N-Boc-4-bromo-indole and selective Boc-deprotection (**2**)

N-Boc-4-bromoindole derivative (5 g, 16.88 mmol, 1 eq), Boc-piperazine (6.28 g, 33.77 mmol, 2 eq), tris(dibenzylideneacetone)dipalladium (310 mg, 0.34 mmol, 0.02 eq). BINAP (420 mg, 0.68 mmol, 0.04 eq) and NaO*t*Bu (1.77 g, 18.38 mmol, 1.5 eq) were solubilized in toluene anhydrous (30 mL) in a 250 mL reaction flask. The flask was evacuated and back filled with argon and the reaction was left stirring at 110°C for 5 h. Then, the mixture was diluted with AcOEt (50 mL) and filtered off on Celite pad and finally concentrated. The crude mixture was purified on silica gel using a mixture of AcOEt/Hex (1/9, *v/v*) as eluting system. Next, the pure intermediate (4.3 g, 10.71 mmol) was dissolved in EtOH (80 mL) and portioned in 4 seal-closed microwave reactors. Each reactor was irradiated for 2 h at 150°C. Then, organic solvent was removed under vacuum and the resulting product (3.07 g, 95% yield) was pure enough for the next synthetic step.

4.1.3. General procedure for benzylation or sulfonilation of the N_1-indole moiety (**3–4**)

A solution of *tert*-butyl 4-(1*H*-indol-4-yl)piperazine-1-carboxylate (1.5 g, 4.98 mmol, 1 eq) in CH_2Cl_2 (20 mL) was cooled to 0°C followed by addition of phosphazene base P_1-*t*-Bu-tris(tetramethylene) (2.27 mL, 7.47 mmol, 1.5 eq). Then, the mixture was treated with 3-chlorobenzyl bromide (0.98 mL, 7.47 mmol, 1.5 eq) or benzenesulfonyl chloride (0.95 mL, 7.47 mmol, 1.5 eq) and stirred for 2 h at rt. After removal of organic solvents, the crude products were purified on silica gel using a mixture of AcOEt/Hex as eluting system.

4.1.4. General procedure for Boc deprotection at piperazine moiety (**5–6**)

Intermediate **3** (1.45 g, 3.4 mmol) was solubilized in CH_2Cl_2 (12 mL) and cooled to 0°C followed by addition of TFA (3 mL). The reaction mixture was stirred for 2 h at rt. Then, the reaction was diluted with CH_2Cl_2 (5 mL) and the acidic excess was carefully neutralized with cold NH_3 aqueous solution till pH = 10. The organic fraction was washed with brine (1 x), dried over anhydrous Na_2SO_4, filtered and concentrated under vacuum. The resulting product **5** was submitted to the next step without further purification. According to the same procedure intermediate **4** was converted into secondary amine **6**.

4.1.5. General procedure for alkylation of phenols (**9–13** and **14–17**)

A suspension of 4-hydroxy-indanone (0.75 g, 5.06 mmol, 1 eq), freshly grinded K_2CO_3 (1.75 g, 12.66 mmol, 2.5 eq) and KOH (0.14 g, 2.53 mmol, 0.5 eq) in 15 ml of acetone. The proper di-bromoalkane (20.24 mmol, 4 eq) was slowly dropped to the reaction mixture and then left stirring at 60 °C overnight. Then, inorganic residues were filtered off, followed by removal of organic solvent under vacuum. The crude products were purified on silica gel using a mixture of AcOEt/Hex as eluting system. to obtain intermediates **9–13**. The same procedure was employed for the alkylation 4-hydroxybenzaldehyde with different di-bromoalkane to achieve intermediates **14–17**.

4.1.6. *General procedure for the alkylation of N_1-functionalized-4-indol-piperazine* (**18–30**)

1-(3-Chlorobenzyl)-4-(piperazin-1-yl)-1*H*-indole **5** (150 mg, 0.46 mmol 1 eq) and freshly grinded K_2CO_3 (190 mg 1.38 mmol, 3 eq) were suspended in 5 ml of acetone, followed by the dropwise addition of the corresponding alkylating agent **9–17** (0.55 mmol, 1.2 eq). The reaction mixture was stirred at 60 °C overnight. Then, inorganic residues were filtered off, followed by removal of organic solvent under vacuum. The crude products were purified on silica gel using a mixture of DCM/MeOH as eluting system, yielding intermediates **18–22** and **25–28**. The same procedure was repeated to obtain intermediates **23–24** and **29–30** by alkylation of 1-((3-chlorophenyl)sulfonyl)-4-(piperazin-1-yl)-1*H*-indole with synthesized alkylating agents **11–12** and **15–16**, respectively.

4.1.7. *General procedure for reductive amination of ketone with propargyl amine* (**31–37**)

Ketone derivative **18** (120 mg, 0.2 mmol, 1 eq), and propargyl amine (26 µL, 0.4 mmol, 2 eq) were solubilized in anhydrous THF (3 mL) and the mixture was stirred for 5 h. The, the reducing agent STAB (127 mg, 0.6 mmol, 3 eq) was added and the mixture was left stirring for additional 2 h. Subsequently, the reaction was quenched with a saturated solution of $NaHCO_3$, washed with H_2O (2 ×), brine (1 ×), dried over Na_2SO_4, filtered and concentrated. The obtained crude product was purified using silica gel with CH_2Cl_2/MeOH as an eluting system to obtain final compound **31**. The same procedure was applied to intermediates **19–24** and for yielding final compounds **32–37**.

4.1.8. *General procedure for reductive amination of benzaldehyde with L-alanamide* (**38–43**)

Benzaldehyde derivative **25** (120 mg, 0.25 mmol, 1 eq), and *L*-alanamide hydrochloride (76 mg, 0.5 mmol, 2 eq) were solubilized in anhydrous THF (3 mL) and the mixture was stirred for 5 h. The, the reducing agent STAB (158 mg, 0.75 mmol, 3 eq) was added and the mixture was left stirring for additional 2 h. Subsequently, the reaction was quenched with a saturated solution

of $NaHCO_3$, washed with H_2O (2 ×), brine (1 ×), dried over Na_2SO_4, filtered and concentrated. The obtained crude product was purified using silica gel with $CH_2Cl_2/MeOH$ as an eluting system to obtain final compound **38**. The same procedure was applied to intermediates **26–30** for yielding final compounds **39–43**.

4.1.9. General procedure for reductive amination of benzaldehyde with N-methyl-propargyl amine (**44–48**)

Benzaldehyde derivative **26** (120 mg, 0.24 mmol, 1 eq), and *N*-methylpropargyl amine (40 µL, 0.48 mmol, 2 eq) were solubilized in CH_2Cl_2 (3 mL) and the mixture was stirred for 30 min. The, the reducing agent STAB (152 mg, 0.72 mmol, 3 eq) was added and the mixture was left stirring for additional 1 h. Subsequently, the reaction was quenched with a saturated solution of $NaHCO_3$, washed with H_2O (2 ×), brine (1 ×), dried over Na_2SO_4, filtered and concentrated. The obtained crude product was purified using silica gel with $CH_2Cl_2/MeOH$ as an eluting system to yield final compound **44**. The same procedure was applied to intermediates **26–30** for yielding final compounds **45–48**.

4.1.10. Characterization data for selected final compounds

4.1.10.1. 4-(4-(4-(1-(3-Chlorobenzyl)-1H-indol-4-yl)piperazin-1-yl)butoxy)-N-(prop-2-yn-1-yl)-2,3-dihydro-1H-inden-1-amine (**33**)

Brown oil, 76 mg (isolated yield 59%) following chromatographic purification over silica gel with $CH_2Cl_2/MeOH$ (9/1, *v/v*); UPLC/MS purity 98%, t_R = 5.14, $C_{35}H_{39}ClN_4O$, MW 567.17, Monoisotopic Mass 566.28, $[M+H]^+$ 567.4. ^1H NMR (500 MHz, $CDCl_3$) δ ppm 1.27 (m, 2H, N-CH_2-C*H₂*), 1.38–1.44 (m, 1H, *indane*), 1.72–1.80 (m, 2H, O-CH_2-C*H₂*), 1.81–1.91 (m, 3H, *indane*), 2.25 (t, *J* = 2.4 Hz, 1H, C*H*≡C-CH_2), 2.55 (t, *J* = 7.3 Hz, 2H, N-C*H₂*-CH_2), 2.70–2.82 (m, 4H, *piperazine*), 3.29–3.34 (m, 4H, *piperazine*), 3.51 (dd, *J* = 5.3, 2.4 Hz, 2H, NH-C*H₂*-C≡CH), 4.02 (t, *J* = 6.2 Hz, 2H, O-C*H₂*-CH_2), 4.42 (dd, *J* = 6.9, 5.2 Hz, 1H, C*H*-NH-CH_2), 5.26 (s, 2H, N-C*H₂*-Ar), 6.56 (dd, *J* = 2.6, 0.9 Hz, 1H, Ar-H), 6.61 (d, *J* = 7.4 Hz, 1H, Ar-H), 6.73 (d, *J* = 8.3 Hz, 1H, Ar-H), 6.88–6.97 (m, 3H, Ar-H), 7.04–7.12 (m, 3H, Ar-H), 7.14–7.23 (m, 3H, Ar-H). ^{13}C NMR (126 MHz, $CDCl_3$) δ ppm 23.6 (N-CH_2-*CH₂*), 27.3 (*CH₂-indane*), 27.5 (O-CH_2-*CH₂*), 33.1 (*CH₂-indane*), 36.2 (NH-*CH₂*-C), 49.7 (N-*CH₂*-Ar), 51.3 (*piperazine*), 53.6 (*piperazine*), 58.5 (N-*CH₂*-CH_2), 62.4 (*CH-indane*), 67.7 (O-CH_2-CH_2), 71.5 (CH_2-C≡*CH*), 82.6 (CH_2-*C*≡CH), 100.8, 104.4, 106.9, 110.2, 116.5, 122.0, 122.8, 124.9, 126.7, 126.8, 127.9, 130.1, 131.8, 134.8, 137.5, 139.8, 145.9, 146.5, 155.7.

4.1.10.2.(S)-2-((4-((6-(4-(1-(3-Chlorobenzyl)-1H-indol-4-yl)piperazin-1-yl)hexyl)oxy)benzyl) amino)propanamide (**41**)

Pale yellow oil, 87 mg (isolated yield 64%) following chromatographic purification over silica gel with CH_2Cl_2/MeOH (9/1, *v/v*); UPLC/MS purity 97%, t_R = 4.61, $C_{35}H_{44}ClN_5O_2$, MW 602.22, Monoisotopic Mass 601.32, [M+H]$^+$ 602.3. ^{1}H NMR (500 MHz, DMSO-d_6) δ ppm 1.08 (d, *J* = 6.9 Hz, 3H, NH-CH-C*H$_3$*), 1.28−1.36 (m, 2H, N-CH$_2$-CH$_2$-C*H$_2$*), 1.36−1.42 (m, 2H, O-CH$_2$-CH$_2$-C*H$_2$*), 1.42−1.49 (m, 2H, N-CH$_2$-C*H$_2$*), 1.63−1.71 (m, 2H, O-CH$_2$-C*H$_2$*), 2.32 (t, *J* = 7.2 Hz, 2H, N-C*H$_2$*-CH$_2$), 2.54 (br. s., 4H, *piperazine*), 2.96 (q, *J* = 6.9 Hz, 1H, NH-C*H*-CH$_3$), 3.07 (br. s., 4H, *piperazine*), 3.43 (d, *J* = 13.2 Hz, 1H, Ar-C*H$_{1a}$*-NH), 3.56 (d, *J* = 13.2 Hz, 1H, Ar-C*H$_{1b}$*-NH), 3.89 (t, *J* = 6.6 Hz, 2H, O-C*H$_2$*-CH$_2$), 5.35 (s, 2H, N-C*H$_2$*-Ar), 6.40 (d, *J* = 3.4 Hz, 1H, Ar-H), 6.43 (d, *J* = 7.5 Hz, 1H, Ar-H), 6.80−6.84 (m, 2H, CO-N*H$_2$*), 6.91−6.97 (m, 2H, Ar-H), 6.99−7.03 (m, 1H, Ar-H), 7.07 (d, *J* = 6.9 Hz, 1H, Ar-H), 7.15−7.21 (m, 3H, Ar-H), 7.24−7.31 (m, 3H, Ar-H), 7.39 (d, *J* = 2.9 Hz, 1H, Ar-H). ^{13}C NMR (126 MHz, DMSO-d_6) δ ppm 19.8 (*C*H$_3$-CH-NH), 26.1 (N-CH$_2$-CH$_2$-*C*H$_2$), 26.8 (O-CH$_2$-CH$_2$-*C*H$_2$), 27.3 (N-CH$_2$-*C*H$_2$), 29.3 (O-CH$_2$-*C*H$_2$), 49.0 (N-*C*H$_2$-Ar), 51.0 (N-*C*H$_2$-CH$_2$), 51.4 (*piperazine*), 53.7 (*piperazine*), 56.9 (NH-*C*H-CH$_3$), 58.5 (O-*C*H$_2$-CH$_2$), 67.9 (Ar-*C*H$_2$-NH), 100.7, 104.9, 106.6, 114.6, 121.8, 122.6, 126.2, 127.2, 127.8, 129.7, 131.0, 132.7, 133.7, 137.3, 141.5, 146.1, 158.1, 177.4 (C=O).

4.1.10.3.(S)-2-((4-(4-(4-(1-(Phenylsulfonyl)-1H-indol-4-yl)piperazin-1-yl)butoxy)benzyl) amino)propanamide (**42**)

Pale yellow oil, 82 mg (isolated yield 60%) following chromatographic purification over silica gel with CH_2Cl_2/MeOH (9/1, *v/v*); UPLC/MS purity 96%, t_R = 4.41, $C_{32}H_{39}N_5O_4S$, MW 589.76, Monoisotopic Mass 589.27, [M+H]$^+$ 590.4. ^{1}H NMR (500 MHz, CDCl$_3$) δ ppm 1.35 (d, *J* = 6.9 Hz, 3H, NH-CH-C*H$_3$*), 1.67–1.76 (m., 2H, N-CH$_2$-C*H$_2$*), 1.78–1.86 (m, 2H, O-CH$_2$-C*H$_2$*), 2.51 (t, *J* = 6.3 Hz, 2H, N-C*H$_2$*-CH$_2$), 2.68 (br. s., 4H, *piperazine*), 3.15 (br. s., 4H, *piperazine*), 3.22 (q, *J* = 6.3 Hz, 1H, NH-C*H*-CH$_3$), 3.63–3.74 (m, 2H, Ar-C*H$_2$*-NH), 3.97 (t, *J* = 6.0 Hz, 2H, O-C*H$_2$*-CH$_2$), 5.59 (br.s., 1H, CO-N*H$_{1a}$*), 6.66 (d, *J* = 4.0 Hz, 1H, Ar-H), 6.71 (d, *J* = 7.4 Hz, 1H, Ar-H), 6.82–6.87 (m, 2H, Ar-H), 7.09 (br.s., 1H, CO-N*H$_{1b}$*), 7.15–7.23 (m, 3H, Ar-H), 7.38–7.43 (m, 2H, Ar-H), 7.46–7.55 (m, 2H, Ar-H), 7.63 (d, *J* = 8.0 Hz, 1H, Ar-H), 7.85 (d, *J* = 7.4 Hz, 2H, Ar-H). ^{13}C NMR (126 MHz, CDCl$_3$) δ ppm 19.8 (*C*H$_3$-CH-NH), 23.4 (N-CH$_2$-*C*H$_2$), 27.3 (O-CH$_2$-*C*H$_2$), 29.8 (*piperazine*), 51.5 (*piperazine*), 52.1 (N-*C*H$_2$-CH$_2$), 53.5 (*piperazine*), 57.7 (NH-*C*H-CH$_3$), 58.3 (O-*C*H$_2$-CH$_2$), 67.8 (Ar-*C*H$_2$-NH), 107.5, 108.0, 110.9, 114.6, 124.2, 124.9, 125.6, 126.9, 129.3, 131.6, 133.9, 136.0, 138.3, 146.1, 158.4, 178.2 (C=O).

4.1.10.4.N-(4-((5-(4-(1-(3-Chlorobenzyl)-1H-indol-4-yl)piperazin-1-yl)pentyl)oxy)benzyl)-N-
methylprop-2-yn-1-amine (**45**)

Pale yellow oil, 99 mg (isolated yield 75%) following chromatographic purification over silica gel with CH_2Cl_2/MeOH (9/0.7, *v/v*); UPLC/MS purity 100%, t_R = 5.73, $C_{35}H_{41}ClN_4O$, MW 569.19, Monoisotopic Mass 568.30, [M+H]$^+$ 569.4. ^1H NMR (500 MHz, CDCl$_3$) δ ppm 1.47–1.56 (m, 2H, O-CH$_2$-CH$_2$-C*H$_2$*), 1.61–1.70 (m, 2H, N-CH$_2$-C*H$_2$*), 1.79–1.86 (m, 2H, O-CH$_2$-C*H$_2$*), 2.23–2.28 (m, 1H, C*H*≡C-CH$_2$), 2.33 (s, 3H, N-C*H$_3$*), 2.46–2.54 (m, 2H, N-C*H$_2$*-CH$_2$), 2.74 (br. s, 4H, *piperazine*), 3.28 (d, *J* = 2.3 Hz, 2H, N-C*H$_2$*-C≡CH), 3.32 (br. s, 4H, *piperazine*), 3.50 (s, 2H, CH$_3$-N-C*H$_2$*-Ar), 3.96 (t, *J* = 6.4 Hz, 2H, O-C*H$_2$*-CH$_2$), 5.25 (s, 2H, N-C*H$_2$*-Ar), 6.56 (d, *J* = 3.2 Hz, 1H, Ar-H), 6.59–6.62 (m, 1H, Ar-H), 6.85 (d, *J* = 8.6 Hz, 2H, Ar-H), 6.91 (dd, *J* = 10.9, 7.2 Hz, 2H, Ar-H), 7.04–7.11 (m, 3H, Ar-H), 7.16–7.27 (m, 4H, Ar-H). ^{13}C NMR (126 MHz, CDCl$_3$) δ ppm 24.2 (N-CH$_2$-CH$_2$-C*H$_2$*), 26.7 (N-CH$_2$-C*H$_2$*), 29.3 (*piperazine*), 29.8 (*piperazine*), 30.4 (O-CH$_2$-C*H$_2$*), 41.8 (N-C*H$_3$*), 44.7 (N-C*H$_2$*-CH$_2$), 49.7 (N-C*H$_2$*-Ar), 51.3 (*piperazine*), 53.7 (*piperazine*), 58.8 (O-C*H$_2$*-CH$_2$), 59.4 (Ar-C*H$_2$*-N-CH$_3$), 67.9 (C*H$_2$*-C≡CH), 73.4 (CH$_2$-C≡*C*H), 78.7 (CH$_2$-*C*≡CH), 100.8, 104.4, 106.9, 114.4, 122.1, 122.8, 124.9, 126.7, 126.8, 127.9, 130.1, 130.3, 130.5, 134.8, 137.5, 139.8, 145.9, 158.4.

4.1.10.5.N-Methyl-N-(4-(4-(4-(1-(phenylsulfonyl)-1H-indol-4-yl)piperazin-1-yl)butoxy)
benzyl)prop-2-yn-1-amine (**47**)

Pale yellow oil, 100 mg (isolated yield 75%) following chromatographic purification over silica gel with CH_2Cl_2/MeOH (9/0.7, *v/v*); UPLC/MS purity 97%, t_R = 4.49, $C_{33}H_{38}N_4O_3S$, MW 570.75, Monoisotopic Mass 570.27, [M+H]$^+$ 571.4. ^1H NMR (500 MHz, CDCl$_3$) δ ppm 1.67–1.75 (m, 2H, N-CH$_2$-C*H$_2$*), 1.79–1.85 (m, 2H, O-CH$_2$-C*H$_2$*), 2.25 (t, *J* = 2.3 Hz, 1H, C*H*≡C-CH$_2$), 2.31 (s, 3H, N-C*H$_3$*), 2.49 (t, *J* = 7.4 Hz, 2H, N-C*H$_2$*-CH$_2$), 2.58–2.74 (m, 4H, *piperazine*), 3.15 (t, *J* = 4.3 Hz, 4H, *piperazine*), 3.27 (d, *J* = 2.3 Hz, 2H, N-C*H$_2$*-C≡CH), 3.49 (s, 2H, CH$_3$-N-C*H$_2$*-Ar), 3.97 (t, *J* = 6.3 Hz, 2H, O-C*H$_2$*-CH$_2$), 6.67 (dd, *J* = 3.7, 0.9 Hz, 1H, Ar-H), 6.71 (d, *J* = 7.7 Hz, 1H, Ar-H), 6.82–6.86 (m, 2H, Ar-H), 7.18–7.26 (m, 3H, Ar-H), 7.37–7.45 (m, 2H, Ar-H), 7.48–7.53 (m, 2H, Ar-H), 7.64 (d, *J* = 8.3 Hz, 1H, Ar-H), 7.83–7.88 (m, 2H, Ar-H). ^{13}C NMR (126 MHz, CDCl$_3$) δ ppm 23.5 (N-CH$_2$-C*H$_2$*), 27.4 (O-CH$_2$-C*H$_2$*), 41.8 (N-C*H$_3$*), 44.7 (N-C*H$_2$*-CH$_2$), 51.6 (*piperazine*), 53.5 (*piperazine*), 58.4 (O-C*H$_2$*-CH$_2$), 59.4 (Ar-C*H$_2$*-N-CH$_3$), 67.7 (C*H$_2$*-C≡CH), 73.4 (CH$_2$-C≡*C*H), 78.7 (CH$_2$-*C*≡CH), 107.6, 107.9, 110.9, 114.4, 124.3, 124.8, 125.6, 126.9, 129.3, 130.4, 133.9, 136.0, 138.3, 146.2, 158.4.

4.1.10.6.N-Methyl-N-(4-((5-(4-(1-(phenylsulfonyl)-1H-indol-4-yl)piperazin-1-yl)pentyl)oxy)

benzyl)prop-2-yn-1-amine (**48**)

Pale yellow oil, 103 mg (isolated yield 78%) following chromatographic purification over silica gel with CH_2Cl_2/MeOH (9/0.7, *v/v*); UPLC/MS purity 100%, t_R = 4.61, $C_{33}H_{38}N_4O_3S$, MW 584.78, Monoisotopic Mass 584.28, [M+H]$^+$ 585.5. ^{1}H NMR (500 MHz, CDCl$_3$) δ ppm 1.48−1.56 (m, 2H, O-CH$_2$-CH$_2$-C*H$_2$*), 1.60−1.67 (m, 2H, N-CH$_2$-C*H$_2$*), 1.79−1.86 (m, 2H, O-CH$_2$-C*H$_2$*), 2.28 (t, *J* = 2.6 Hz, 1H, C*H*≡C-CH$_2$), 2.33 (s, 3H, N-C*H$_3$*), 2.47 (t, *J* = 7.4 Hz, 2H, N-C*H$_2$*-CH$_2$), 2.68 (br. s., 4H, *piperazine*), 3.18 (t, *J* = 4.6 Hz, 4H, *piperazine*), 3.29 (d, *J* = 2.3 Hz, 2H, N-C*H$_2$*-C≡CH), 3.51 (s, 2H, CH$_3$-N-C*H$_2$*-Ar), 3.96 (t, *J* = 6.3 Hz, 2H, O-C*H$_2$*-CH$_2$), 6.68−6.70 (m, 1H, Ar-H), 6.73 (d, *J* = 7.5 Hz, 1H, Ar-H), 6.83−6.87 (m, 2H, Ar-H), 7.20−7.26 (m, 3H, Ar-H), 7.40−7.44 (m, 2H, Ar-H), 7.50−7.53 (m, 1H, Ar-H), 7.53 (d, *J* = 3.4 Hz, 1H, Ar-H), 7.66 (d, *J* = 8.6 Hz, 1H, Ar-H), 7.86−7.87 (m, 1H, Ar-H), 7.88−7.89 (m, 1H, Ar-H). ^{13}C NMR (126 MHz, CDCl$_3$) δ ppm 24.2 (N-CH$_2$-CH$_2$-*C*H$_2$), 26.6 (N-CH$_2$-*C*H$_2$), 29.3 (O-CH$_2$-*C*H$_2$), 41.7 (N-*C*H$_3$), 44.7 (N-*C*H$_2$-CH$_2$), 51.5 (*piperazine*), 53.5 (*piperazine*), 58.7 (O-*C*H$_2$-CH$_2$), 59.4 (Ar-*C*H$_2$-N-CH$_3$), 67.8 (*C*H$_2$-C≡CH), 73.4 (CH$_2$-C≡*C*H), 78.7 (CH$_2$-*C*≡CH), 107.6, 108.0, 110.9, 114.4, 124.3, 124.9, 125.6, 126.9, 129.3, 130.3, 130.5, 133.9, 136.0, 138.3, 146.2, 158.4. Anal. calcd for dihydrochloride dihydrate salt $C_{33}H_{38}N_4O_3S \cdot 2HCl \cdot 2H_2O$: C: 58.87, H: 6.68, N: 8.08, S: 4.62; Found C: 59.03, H: 6.44, N: 7.72, S: 4.39. M.p. for $C_{33}H_{38}N_4O_3S \cdot 2HCl \cdot 2H_2O$: 215.1–219.3°C.

4.2. In silico simulations

4.2.1. Molecular docking

The 5-HT$_6$R homology models were obtained according to the procedure described before on the β$_2$ receptor template and successfully used in our earlier studies of different groups of 5-HT$_6$R ligands simulations.[48,49] The structure of monoamine oxidases B (PDB code 2C65)[38] in complex with irreversible inhibitor rasagilline analog (4-(N-methyl-N-ethyl-carbamoyloxy)-N-methyl-N-propargyl-1(R)-aminoindan) was fetched from the Protein Data Bank. The structures of the 5-HT$_6$ receptor and MAO-B enzyme were optimized using the induced-fit docking (IFD) procedure from Schrödinger Suite. The IFD combines flexible ligand docking with target structure prediction and side chain refinement. The structure of **48** was used as input to IFD. Centroid of the grid box was anchored on D3.32 and I199 in 5-HT$_6$ and MAO-B, respectively. Due to the size of the input ligand, it allowed on residue refinement within 12 Å and 33 Å of ligand poses for 5-HT$_6$ and MAO-B, respectively. The Extended Sampling Protocol was used, which generates up to 80 poses per ligand by automated docking. All obtained L–R

complexes were inspected visually to select those that displayed the closest compliance with the common binding mode for studied protein targets. Final validation of the selected conformations was performed by docking (Glide SP mode) the designed library, retaining only those with a coherent binding mode.[50] The 3-dimensional structures of the ligands were obtained using LigPrep v3.6,[51] and the appropriate ionization states at pH = 7.4±1.0 were assigned using Epik v3.4.[52]

4.2.2. QM/MM Optimization

The L–R complexes selected in IFD procedure were next optimized using QM/MM approach using QSite. The QM region contained ligand and amino acid side chain directly interacting with the ligand was described by a combination of DFT hybrid functional B3LYP and LACVP* basis set, while the rest of the system was optimized using OPLS2005 force field.

4.2.3. Covalent docking

The CovDock workflow[53] from Schrodinger Suite was used for pose prediction and scoring of covalently bound ligands to a flavin adenine dinucleotide cofactor (FAD) presence in catalytic site of MAO-B enzyme. The reaction between FAD and propargyl group was not pre-defined in CovDock library, thus we used custom reaction editor to describe the reaction based on the mechanism proposed by Tandarić et al.[39] At first, we defined in SMARTS language the fragments of the ligand [C#CC[N,n]] and FAD [[nH]c(=O)cNc] between which the reaction occurs. The grid center was set to I199, assuming its size to 33 Å. The rest setting was used as default.

4.3. In vitro *pharmacological evaluation*

4.3.1. Radioligand binding assays

All experiments were carried out according to the previously published procedures.[54–56] HEK293 cells stably expressing human 5-HT$_{1A}$, 5-HT$_6$, 5-HT$_{7b}$ and D$_{2L}$ receptors (prepared with the use of Lipofectamine 2000) or CHO-K1 cells with plasmid containing the sequence coding for the human serotonin 5-HT$_{2A}$ receptor (Perkin Elmer) were maintained at 37 °C in a humidified atmosphere containing 5% CO$_2$ and grown in Dulbecco's Modified Eagle's Medium containing 10% dialyzed fetal bovine serum and 500 µg/ml G418 sulfate. For membrane preparation, cells were cultured in 150 cm^2 flasks, grown to 90% confluence, washed twice

with pre-warmed to 37 °C phosphate buffered saline (PBS) and centrifuged (200 × g) in PBS containing 0.1 mM EDTA and 1 mM dithiothreitol. Prior to membrane preparation, pellets were stored at -80 °C.

Cell pellets were thawed and homogenized in 10 volumes of assay buffer using an Ultra Turrax tissue homogenizer and centrifuged twice at 35,000 × g for 15 min at 4 °C, with incubation for 15 min at 37 °C between the centrifugations. The composition of the assay buffers was experimentally selected to achieve the maximum signal window (more details in SI). All assays were carried out in a total volume of 200 μL in 96-well plates for 1 h at 37 °C, except 5-HT$_{1A}$R and 5-HT$_{2A}$R which were incubated at room temperature and 27 °C, respectively. The process of equilibration was terminated by rapid filtration through Unifilter plates with a 96-well cell harvester and radioactivity retained on the filters was quantified on a Microbeta plate reader (PerkinElmer, USA). For displacement studies the assay samples contained as radioligands (PerkinElmer, USA): 2.5 nM [^{3}H]-8-OH-DPAT (135.2 Ci/ mmol) for 5-HT$_{1A}$R; 1 nM [^{3}H]-ketanserin (53.4 Ci/mmol) for 5-HT$_{2A}$R; 2 nM [^{3}H]-LSD (83.6 Ci/mmol) for 5-HT$_6$R; 0.8 nM [^{3}H]-5-CT (39.2 Ci/mmol) for 5-HT$_7$R or 2.5 nM [^{3}H]-raclopride (76.0 Ci/mmol) for D$_{2L}$R. Non-specific binding was defined in the presence of 10 μM of 5-HT in 5-HT$_{1A}$R and 5-HT$_7$R binding experiments, whereas 20 μM of mianserin, 10 μM of methiothepine or 10 μM of haloperidol were used in 5-HT$_{2A}$R, 5-HT$_6$R and D$_{2L}$ assays, respectively. Each compound was tested in triplicate at 7 concentrations (10^{-10}-10^{-4} M). The inhibition constants (K_i) were calculated from the Cheng-Prusoff equation.[57]

Additionally, the affinity of compound **48** and α$_1$ and β$_1$-adrenergic receptors, histaminic H$_1$ and muscarinic M$_1$ receptors were evaluated at Eurofins. The results were expressed as the % inhibition of the control binding according to experimental protocols described online at https://www.eurofins.com/.

4.3.2. Monoamine Oxidase Assays

Inhibition activity of evaluated compounds was measured using human recombinant MAO-B and MAO-A (Sigma Aldrich M7441 and M7316) in the fluorometric method for detecting monoamine oxidase activity. The assay was carried out in 96-well plate. 2 μL of appropriate concentration of tested compounds in DMSO were added to wells that contained 98 μL of enzyme dilution (0.53 U/ml) in phosphate buffer (50 mM, pH 7.4). After the 30 minutes of preincubation in room temperature 50 μL of the solution of 800 μM 10-Acetyl-3,7-dihydroxyphenoxazine (Cayman Chemical Company 10010469) and 4 U/mL horse radish

peroxidase (HRP, Sigma Aldrich P6782) was added and enzymatic reaction was started by addition of 50 μL of 800 μM p-tyramine (Alfa Aesar A12220) solution. The signal was measured after 1h (excitation at 570 nm and emission at 585 nm) using EnSpire® multimode plate reader (Perkin Elmer, Inc.). Rasagiline (1 μM) or clorgyline (1 μM) were tested as reference compounds for MAO-B and MAO-A inhibitions, respectively.[58,59]

4.3.3. Reversibility studies

To investigate reversibility of MAO-B inhibition compound **48**, rasagiline and safinamide were tested in concentration corresponding to their IC_{80} values. Experiment was carried out in 96-well plate divided into two parts. In the first portion hMAO-B was incubated with inhibitors for 30 minutes. In the second portion of inhibitors were added to hMAO-B directly before the next step. Then 10 μM p-tyramine and the solution of 800 μM 10-acetyl-3,7-dihydroxyphenoxazine and 4 U/mL HRP were added to both parts of the plate. Fluorescence signal had been measured in the microplate reader for 22 minutes then the concentration of p-tyramine was increased to 1 mM. After addition of p-tyramine fluorescence was measured every 5 minutes for 5 hours.[59]

4.3.4. Determination of cAMP production in 1321N1 cells

The properties of compound **48** to inhibit cAMP production induced by 5-CT (1000 nM), a 5-HT_6R agonist, was evaluated. Compounds were tested in triplicate at 8 concentrations (10^{-11}–10^{-4} M). The level of cAMP was measured using frozen recombinant 1321N1 cells expressing the Human Serotonin 5-HT_6R (PerkinElmer). Total cAMP was measured using the LANCE cAMP detection kit (PerkinElmer), according to the manufacturer's recommendations. For quantification of cAMP levels, 2000 cells/well (5 μL) were incubated with mixture of compounds (5 μL) for 30 min at room temperature in 384-well white opaque microtiter plate. After incubation, the reaction was stopped and cells were lysed by the addition of 10 μL of working solution (5 μL Eu-cAMP and 5 μL ULight-anti-cAMP) for 1 h at room temperature. Time-resolved fluorescence resonance energy transfer (TR-FRET) was detected by an Infinite M1000 Pro (Tecan) using instrument settings from LANCE cAMP detection kit manual. K_b values were calculated from Cheng–Prusoff equation specific for the analysis of functional inhibition curves: $K_b = IC_{50}/(1+A/EC_{50})$ where A represents agonist concentration, IC_{50} the

concentration of antagonist producing a 50% reduction in the response to agonist, and EC_{50} the agonist concentration which causes a half of the maximal response.[57]

4.3.5. Determination of cAMP production in NG108-15 cells

NG108-15 cells were grown in Dulbecco's modified Eagle's medium (DMEM) supplemented with 10% dialyzed fetal calf serum, 2% hypoxanthine/aminopterin/thymidine (Life technologies), and antibiotics. cAMP measurement was performed in cells transiently expressing $5\text{-}HT_6R$ using the bioluminescence resonance energy transfer (BRET) sensor for cAMP, CAMYEL (cAMP sensor using YFP-Epac-RLuc).[60] NG108-15 cells were co-transfected in suspension with $5\text{-}HT_6R$ (0.5 µg DNA/million cells) and CAMYEL constructs (1 µg DNA/million cells), using Lipofectamine 2000, according to the manufacturer's protocol, and plated in white 96-well plates (Greiner), at a density of 50,000 cells per well. Twenty-four h after transfection, cells were washed with PBS containing calcium and magnesium. To test the inverse agonist properties of compound **48** and intepirdine, cells were treated with vehicle or with the tested compound at incremental concentrations of these compounds (from 0.1 nM to 10 µM). Coelanterazine H (Molecular Probes) was added at a final concentration of 5 µM, and left at room temperature for 5 min. BRET was measured using a Mithras LB 940 plate reader (Berthold Technologies). Expression of $5\text{-}HT_6R$ in NG108-15 cells induced a strong decrease in CAMYEL BRET signal, compared with cells transfected with an empty vector instead of the plasmid encoding the $5\text{-}HT_6R$. This decrease in CAMYEL BRET signal was thus used as an index of $5\text{-}HT_6R$ constitutive activity at Gs signaling.

4.4. Assessment of preliminary ADME properties

4.4.1. PAMPA – Parallel artificial membrane permeability assay

Parallel artificial membrane permeability assay (PAMPA) was performed using Corning® Gentest™ Pre-coated PAMPA Plate System, according to the manufacturer's instructions. Compound **48** (100 µM) was incubated on plates in phosphate-buffer saline (pH 7.4) for 5 h at room temperature. Concentrations of **48** in donor and acceptor solutions were determined using UPLC-MS with the internal standard based on pentoxifylline method. Membrane permeability expressed as log$P$e was calculated as follows:

$$logPe = log\left(\frac{-\ln\left[1 - C_A\big/\dfrac{C_D \times V_D + C_A \times V_A}{V_D + V_A}\right]}{A \times \left(\dfrac{1}{V_D} + \dfrac{1}{V_A}\right) \times t}\right)$$

where CD and CA are the final concentrations after incubation and VD, VA - volumes of the donor and the acceptor solutions (0.3 ml, 0.2 ml), respectively. *A* - membrane surface area (0.3 cm2),t - incubation time (18 000 s). Two reference standards were used in the study – verapamil (Pe = 1.85 * 10-5 cm/sec) – a well permeable drug and doxorubicin (Pe= ND, not detected in acceptor compartment) – no membrane penetration properties.

4.4.2. In vitro metabolic stability studies

Metabolic stability of tested compound was analyzed using incubation systems, composed of: tested compound (10 µM), rat liver microsomes (RLMs, microsomes from rat male liver, pooled; 0.4 mg/mL; Sigma Aldrich), NADPH-regenerating system (NADP+, glucose-6-phosphate and glucose-6-phosphate dehydrogenase in 100 mM potassium buffer, pH 7.4; all from Sigma Aldrich) and potassium buffer, pH 7.4. Stock solution of tested compounds was prepared in methanol (the final methanol concentration in incubation mixture does not exceed 0,1%). Firstly, all samples contained incubation mixture (without NADPH-regenerating system) were pre-incubated in thermoblock at 37°C, for 10 min. Then reaction was initiated by the addition of NADPH-regenerating system. In control samples NADPH-regenerating system was replaced with potassium buffer. Probes were incubated for 30 and 60 min at 37°C. After addition of internal standard (pentoxifylline, 10 µM) biotransformation process was stopped by addition of perchloric acid. Next, samples were centrifuge and supernatants were analyzed using UPLC/MS (Waters Corporation, Milford, MA). All experiments were run in duplicates. Half-life time was evaluated using non-linear regression model using Graph Pad Prism software and intristinic clearence was calculated from the equation Cl_{int} = (volume of incubation [µl]/protein in the incubation [mg]) 0,693/$t_{1/2}$.[61]

4.4.3. Preliminary in vivo *pharmacokinetics experiments*
4.4.3.1.   Instrumentation and operating conditions

The LC/ESI-MS/MS experiments were performed on an ABSciex (Concord, Ontario, Canada) API 3200 triple quadrupole mass spectrometer equipped with an electrospray (ESI) ionization interface. This instrument was coupled to Shimadzu (Shimadzu, Japan) LC system. Data

acquisition and processing were accomplished using ABSciex Analyst 1.5.2 data collection and integration software.

4.4.3.2. *Chromatographic and Mass spectrometric conditions*

Acclaim Polar Advantage II (3.0 mm x 74 mm, 3 μm, 120A, Dionex, USA) analytical column was used for compound separation. The temperatures of the column thermostat and the autosampler were set at 40°C and 10°C, respectively. The mobile phase consisted of a mixture of acetonitrile with addition of 0.1% formic acid (solvent A) and water with addition of 0.1% formic acid (solvent B) and was set at a flow rate of 0.4 mL/min. Starting amount of solvent A is 10%, isocratic elution from 0 to 5 min, and then gradient up to 90% of solvent A, and maintained to 10 min, and then gradient down to 10% of solvent A, and maintained to 15 min. To find the optimal parameters of ion path and ion source for studied compound the quantitative optimization was done by direct infusion of the molecule at a concentration of 1 μg/mL, and at a flow rate of 10 μL/min using a Hamilton syringe pump (Hamilton, Reno, Nevada). The ion source parameters were as follows: ion spray voltage: 4500 V; nebulizer gas (gas 1): 20 psi; turbo gas (gas 2): 20 psi; temperature of the heated nebulizer: 400°C; curtain gas: 40 psi; collision gas: 6 psi. Mass spectra were acquired by SRM with precursor/predominant product ion transitions for the analyte. The mass spectral Q1→Q3 transitions monitored for compound **48** and for IS were m/z 585.1→516.2 and m/z 305→248, respectively. The peak widths of precursor and product ions were set to 0.7 full width half-height. Quantification was done via peak area ratio.

4.4.3.3. *Sample pretreatment*

The plasma and brain sample pretreatment procedure involved acetonitrile precipitation. A 5 μL aliquot of the internal standard (IS, PH003437, Merck, Darmstadt, Germany). working solution (5 μg/mL) was added to 100 μL of the collected rat plasma sample, which was then vortex-mixed for 10 seconds. Thereafter, 200 μL of acetonitrile was added, vortexed during 20 min, and then centrifuged (10 000 rpm, 10 min). The supernatant (200 μL) was then transferred to insert placed in an autosampler vial, and a 20 μL volume of this was injected onto the LC column. Brain samples were thawed before use, and whole brain were weighted and placed in a glass mortar and pestle tissue grinder, and homogenized with an appropriate amount of phosphate buffer (pH 7.4) in 1:2.5 ratio. Afterward, 100 μL of tissue homogenates were transferred to new Eppendorf tubes and spiked with 5 μL of the internal standard working

solution. All samples were stored on ice during the preparation process and followed by procedures similar to those described above.

4.4.3.4. Animals

A group of 32 adult male rats (Wistar, 200 - 220 g) were used in the experiment. The animals were purchased from the Animal House at the Faculty of Pharmacy, Jagiellonian University Medical College, Krakow, Poland. During the habituation period the groups of 4 rats were kept in a plastic cage at a controlled room temperature ($22\pm2°C$), humidity ($55\pm10\%$), full spectrum cold white light (350–400 lx), on 12 hr light/12 dark cycles (the lights on at 7:00 a.m., and off at 19:00 p.m.), and had free access to standard laboratory pellet and tap water. For pharmacokinetic study compound **48** dissolved in saline were administered by intragastric gavage at a dose of 3 mg/kg. Blood samples were collected at 0 min (predose), 5 min, 15 min, 30 min, 60 min, 120 min, 240 min and 480 min after compound administration. The blood and brain samples were collected under general anesthesia induced by *i.p.* injection of 50 mg/kg ketamine plus 8 mg/kg xylazine. The blood samples were taken into heparinized tubes, immediately centrifuged at 1000xg for 10 min, and plasma was collected. The plasma and brain samples were immediately frozen at −80°C. All experimental procedures were carried out in accordance with EU Directive 2010/63/EU and approved by the I Local Ethics Committee for Experiments on Animals of the Jagiellonian University in Krakow, Poland.

4.5. Assessment of glioprotecting properties
4.5.1. Cell culture

Astrocytes (C8-D1A cells) were cultured in 25 cm^2 flask with DMEM supplemented with 10% FBS at 37 °C, in a humidified atmosphere with 5% CO_2 until the cells reached 80–90% confluence. Cells were harvested and seeded in 96-well plates at a density of 1×10^4 cells per well. They were pre-incubated with tested compounds analyzed compounds for 12 hours, then 6-OHDA (25 µM) was added for next 24 hours. The ability of compounds to prevent 6-OHDA-induced cytotoxicity was assessed by using the MTT and LDH assays.

4.5.2. MTT assay

Cell viability was estimated by using the MTT assay, which assesses the ability mitochondrial dehydrogenases to reduce tetrazolium salts into a colored formazan compound.[62] At the end of the incubation period, 10 µL of MTT (5 mg/mL) were added to each well. After 4 h, formazan crystals were solubilized with DMSO and optical density was measured at 570

nm by using a SpectraMax iD3 Multi-Mode Microplate Reader (Molecular Devices). Each experiment was performed in triplicate and repeated three times.

4.5.3. LDH assay

Cells were seeded at density 3×10^4 cells/per well in 96 well plates. After 24 h selegiline, intepirdine, and compound **48** were added to final concentrations of 0,25 μM. After 24 h pre-incubation, 6-OHDA (25 μM) was added to the cultures for an additional 24-h period to induce astrocyte injury. Then, plates were centrifuged (200 x g, 2 min) and 50 μL of the supernatant were transferred into the corresponding 96-well plate. Subsequently, 50 μL of LDH-reaction mixture prepared according to the manufacturer's instructions (Invitrogen) were added to each well. Incubation was conducted in darkness for 30 min at room temperature. Next, stop solution was added and absorbance was measured at 490 nm (A490) using a plate reader (Spectra Max iD3, Molecular Devices). Cytotoxicity was determined as follows: cytotoxicity (%)=[(compound LDH activity – spontaneous LDH activity)/(maximum LDH activity – spontaneous LDH activity)] × 100. The maximum LDH activity was prepared by treating cells with lysis buffer (control +). The medium used in the LDH assay contained 1% FBS. Three independent experiments were performed for each condition.

4.6. In vivo pharmacological evaluation

The experiments were performed according to the previously reported procedures[63,64] and were conducted in accordance with the NIH Guide for the Care and Use of Laboratory Animals and were approved by the Ethics Committee for Animal Experiments, Institute of Pharmacology. Male Sprague–Dawley rats (Charles River, Germany) weighing ~250 g at the arrival were housed in the standard laboratory cages, under standard colony A/C controlled conditions: room temperature 21 ± 2°C, humidity (40–50 %), 12-hr light/dark cycle (lights on: 06:00) with ad libitum access to food and water. Rats were allowed to acclimatize for at least 7 days before the start of the experimental procedure. During this week animals were handled for at least 3 times. Behavioral testing was carried out during the light phase of the light/dark cycle. At least 1 h before the start of the experiment, rats were transferred to the experimental room for acclimation. Rats were tested in a dimly lit (25 lx) "open field" apparatus made of a dull gray plastic (66 × 56 × 30 cm). After each measurement, the floor was cleaned and dried.

4.6.1. Drug Treatment

Scopolamine hydrobromide used to attenuate learning, was purchase from Sigma Aldrich (Germany). Scopolamine and tested compound **48** were solubilized in distilled water and then administered at the dose of 1.25 mg/kg (*i.p.*) and 1–3 mg/kg (*p.o.*) 30 and 120 min before familiarization phase (T1), respectively.

4.6.2. *Experimental Procedure*

Procedure consisted of habituation to the arena (without any objects) for 5 min, 24 hours before the test and test session comprised of two trials separated by an inter trial interval (ITI). For scopolamine (SCOP)-induced memory impairment paradigm, 1 hour ITI was chosen. During the first trial (familiarization, T1) two identical objects (A1 and A2) were presented in opposite corners, approximately 10 cm from the walls of the open field. In the second trial (recognition, T2) one of the objects was replaced by a novel one (A = familiar and B = novel). Both trials lasted 3 min and animals were returned to their home cage after T1. The objects used were the glass beakers filled with the gravel and the plastic bottles filled with the sand. The heights of the objects were comparable (~12 cm) and the objects were heavy enough not to be displaced by the animals. The sequence of presentations and the location of the objects was randomly assigned to each rat. The animals explored the objects by looking, licking, sniffing or touching the object while sniffing, but not when leaning against, standing or sitting on the object. Any rat spending less than 5 s exploring the two objects within 3 min of T1 or T2 was eliminated from the study. Exploration time of the objects and the distance travelled were measured using the Any-maze® video tracking system. Based on exploration time (E) of two objects during T2, discrimination index (DI) was calculated according to the formula: DI = (EB–EA)/(EA+AB).

Supporting Information Available

Supporting information contains characterization data for all intermediates and final compounds excluded from the main manuscript; MS, ^{1}H-NMR and ^{13}C-NMR spectra for selected final compounds. This material is available free of charge via the Internet.

References:
(1)   De Strooper, B. Lessons from a failed γ-secretase Alzheimer trial. *Cell* **2014**, *159* (4), 721–726.
(2)   Panza, F.; Lozupone, M.; Solfrizzi, V.; Sardone, R.; Piccininni, C.; Dibello, V.; Stallone, R.; Giannelli, G.; Bellomo, A.; Greco, A.; et al. BACE Inhibitors in clinical development for the treatment of Alzheimer's disease. *Expert Rev. Neurother.* **2018**, *18* (11), 847–857.
(3)   Andrews, M.; Tousi, B.; Sabbagh, M. N. 5-HT$_6$ antagonists in the treatment of Alzheimer's dementia: current progress. *Neurol. Ther.* **2018**, *7* (1), 51–58.
(4)   Park, J. H.; Ju, Y. H.; Choi, J. W.; Song, H. J.; Jang, B. K.; Woo, J.; Chun, H.; Kim, H. J.; Shin, S. J.; Yarishkin, O.; et al. Newly developed reversible MAO-B inhibitor circumvents the shortcomings of irreversible inhibitors in Alzheimer's disease. *Sci. Adv.* **2019**, *5* (3), eaav0316.
(5)   Bolognesi, M. L. Polypharmacology in a single drug: multitarget drugs. *Curr. Med. Chem.* **2013**, *20* (13), 1639–1645.
(6)   Bolognesi, M. L. Harnessing polypharmacology with medicinal chemistry. *ACS Med. Chem. Lett.* **2019**, *10* (3), 273–275.
(7)   Jiang, X. Y.; Chen, T. K.; Zhou, J. T.; He, S. Y.; Yang, H. Y.; Chen, Y.; Qu, W.; Feng, F.; Sun, H. P. Dual GSK-3β/AChE inhibitors as a new strategy for multitargeting anti-Alzheimer's disease drug discovery. *ACS Med. Chem. Lett.* **2018**, *9* (3), 171–176.
(8)   Kumar, B.; Kumar, V.; Prashar, V.; Saini, S.; Dwivedi, A. R.; Bajaj, B.; Mehta, D.; Parkash, J.; Kumar, V. Dipropargyl substituted diphenylpyrimidines as dual inhibitors of monoamine oxidase and acetylcholinesterase. *Eur. J. Med. Chem.* **2019**, *177*, 221–234.
(9)   Prati, F.; De Simone, A.; Bisignano, P.; Armirotti, A.; Summa, M.; Pizzirani, D.; Scarpelli, R.; Perez, D. I.; Andrisano, V.; Perez-Castillo, A.; et al. Multitarget drug discovery for Alzheimer's disease: triazinones as BACE-1 and GSK-3β inhibitors. *Angew. Chem. Int. Ed. Engl.* **2015**, *54* (5), 1578–1582.
(10)   Saavedra, O. M.; Karila, D.; Brossard, D.; Rojas, A.; Dupuis, D.; Gohier, A.; Mannoury la Cour, C.; Millan, M. J.; Ortuno, J. C.; Hanessian, S. Design and synthesis of novel N-sulfonyl-2-indoles that behave as 5-HT$_6$ receptor ligands with significant selectivity for D$_3$ over D$_2$ receptors. *Bioorg. Med. Chem.* **2017**, *25* (1), 38–52.
(11)   Grychowska, K.; Chaumont-Dubel, S.; Kurczab, R.; Koczurkiewicz, P.; Deville, C.; Krawczyk, M.; Pietruś, W.; Satała, G.; Buda, S.; Piska, K.; et al. Dual 5-HT$_6$ and D$_3$ Receptor antagonists in a group of 1H-pyrrolo[3,2-c]quinolines with neuroprotective and procognitive Aactivity. *ACS Chem. Neurosci.* **2019**, *10*, 3183–3196.
(12)   Staroń, J.; Kurczab, R.; Warszycki, D.; Satała, G.; Krawczyk, M.; Bugno, R.; Lenda, T.;

Popik, P.; Hogendorf, A. S.; Hogendorf, A.; et al. Virtual screening-driven discovery of dual 5-HT$_6$/5-HT$_{2A}$ receptor ligands with pro-cognitive properties. *Eur. J. Med. Chem.* **2020**, *185*, 111857.

(13) Millan, M. J.; Dekeyne, A.; Gobert, A.; Brocco, M.; la Cour, C.; Ortuno, J. C.; Watson, D.; Fone, K. C. F. Dual-acting agents for improving cognition and real-world function in Alzheimer's disease: focus on 5-HT$_6$ and D$_3$ receptors as hubs. *Neuropharmacology* **2020**, 108099.

(14) Lalut, J.; Karila, D.; Dallemagne, P.; Rochais, C. Modulating 5-HT$_4$ and 5-HT$_6$ receptors in Alzheimer's disease treatment. *Future Med. Chem.* **2017**, *9* (8), 781–795.

(15) Rodríguez-Soacha, D. A.; Scheiner, M.; Decker, M. Multi-Target-Directed-Ligands acting as enzyme inhibitors and receptor ligands. *Eur. J. Med. Chem.* **2019**, *180*, 690–706.

(16) Simoni, E.; Daniele, S.; Bottegoni, G.; Pizzirani, D.; Trincavelli, M. L.; Goldoni, L.; Tarozzo, G.; Reggiani, A.; Martini, C.; Piomelli, D.; et al. Combining galantamine and memantine in multitargeted, new chemical entities potentially useful in Alzheimer's disease. *J. Med. Chem.* **2012**, *55* (22), 9708–9721.

(17) Incerti, M.; Flammini, L.; Saccani, F.; Morini, G.; Comini, M.; Coruzzi, M.; Barocelli, E.; Ballabeni, V.; Bertoni, S. Dual-Acting drugs: an in vitro study of nonimidazole histamine H$_3$ receptor antagonists combining anticholinesterase activity. *ChemMedChem* **2010**, *5* (7), 1143–1149.

(18) Lalut, J.; Santoni, G.; Karila, D.; Lecoutey, C.; Davis, A.; Nachon, F.; Silman, I.; Sussman, J.; Weik, M.; Maurice, T.; et al. Novel multitarget-directed ligands targeting acetylcholinesterase and σ$_1$ receptors as lead compounds for treatment of Alzheimer's disease: synthesis, evaluation, and structural characterization of their complexes with acetylcholinesterase. *Eur. J. Med. Chem.* **2019**, *162*, 234–248.

(19) Lecoutey, C.; Hedou, D.; Freret, T.; Giannoni, P.; Gaven, F.; Since, M.; Bouet, V.; Ballandonne, C.; Corvaisier, S.; Malzert Fréon, A.; et al. Design of donecopride, a dual serotonin subtype 4 receptor agonist/acetylcholinesterase inhibitor with potential interest for Alzheimer's disease treatment. *Proc. Natl. Acad. Sci.* **2014**, *111* (36), 3825–3830.

(20) Więckowska, A.; Kołaczkowski, M.; Bucki, A.; Godyń, J.; Marcinkowska, M.; Więckowski, K.; Zaręba, P.; Siwek, A.; Kazek, G.; Głuch-Lutwin, M.; et al. Novel Multi-Target-Directed Ligands for Alzheimer's disease: combining cholinesterase inhibitors and 5-HT$_6$ receptor antagonists. Design, synthesis and biological evaluation. *Eur. J. Med. Chem.* **2016**, *124*, 63–81.

(21) Youn, Y. H.; Han, Y. G. Primary cilia in brain development and diseases. *Am. J. Pathol.* **2018**, *188* (1), 11–22.

(22) Lesiak, A. J.; Brodsky, M.; Cohenca, N.; Croicu, A. G.; Neumaier, J. F. Restoration of physiological expression of 5-HT$_6$ receptor into the primary cilia of null mutant neurons lengthens both primary cilia and dendrites. *Mol. Pharmacol.* **2018**, *94* (1), 731–742.

(23) Park, S. M.; Jang, H. J.; Lee, J. H. Roles of primary cilia in the developing brain. *Frontiers in Cellular Neurosc.* **2019**, p 218.

(24) Chaumont-Dubel, S.; Dupuy, V.; Bockaert, J.; Becamel, C.; Marin, P. The 5-HT$_6$ receptor interactome: new insight in receptor signaling and its impact on brain physiology and pathologies. *Neuropharmacology* **2019**, *172*, 107839.

(25)   Codony, X.; Vela, J. M.; Ramírez, M. J. 5-HT$_6$ Receptor and cognition. *Curr. Opin. Pharmacol.* **2011**, *11* (1), 94–100.

(26)   de Jong, I. E. M.; Mørk, A. Antagonism of the 5-HT$_6$ receptor – preclinical rationale for the treatment of Alzheimer's disease. *Neuropharmacology* **2017**, *125* (Supplement C), 50–63.

(27)   Ivachtchenko, A. V; Lavrovsky, Y.; Ivanenkov, Y. A. AVN-211, Novel and highly selective 5-HT$_6$ receptor small molecule antagonist, for the treatment of Alzheimer's Disease. *Mol. Pharm.* **2016**, *13* (3), 945–963.

(28)   Vanda, D.; Soural, M.; Canale, V.; Chaumont-Dubel, S.; Satała, G.; Kos, T.; Funk, P.; Fülöpová, V.; Lemrová, B.; Koczurkiewicz, P.; et al. Novel non-sulfonamide 5-HT$_6$ receptor partial inverse agonist in a group of imidazo[4,5-b]pyridines with cognition enhancing properties. *Eur. J. Med. Chem.* **2018**, *144*, 716–729.

(29)   Hogendorf, A. S.; Hogendorf, A.; Kurczab, R.; Kalinowska-Tluscik, J.; Popik, P.; Nikiforuk, A.; Krawczyk, M.; Satala, G.; Lenda, T.; Knutelska, J.; et al. 2-Aminoimidazole-based antagonists of the 5-HT$_6$ receptor - a new concept in aminergic GPCR ligand design. *Eur. J. Med. Chem.* **2019**, *179*, 1–15.

(30)   Morozova, M. A.; Lepilkina, T. A.; Rupchev, G. E.; Beniashvily, A. G.; Burminskiy, D. S.; Potanin, S. S.; Bondarenko, E. V; Kazey, V. I.; Lavrovsky, Y.; Ivachtchenko, A. V. Add-on clinical effects of selective antagonist of 5HT$_6$ receptors AVN-211 (CD-008-0173) in patients with schizophrenia stabilized on antipsychotic treatment: pilot study. *CNS Spectr.* **2014**, *19* (4), 316–323.

(31)   Schedin-Weiss, S.; Inoue, M.; Hromadkova, L.; Teranishi, Y.; Yamamoto, N. G.; Wiehager, B.; Bogdanovic, N.; Winblad, B.; Sandebring-Matton, A.; Frykman, S.; et al. Monoamine Oxidase B is elevated in Alzheimer Disease neurons, is associated with γ-secretase and regulates neuronal amyloid β-peptide levels. *Alzheimers. Res. Ther.* **2017**, *9* (1), 57.

(32)   Ramsay, R. R. Molecular aspects of Monoamine Oxidase B. *Prog. Neuropsychopharmacol. Biol. Psychiatry* **2016**, *69*, 81–89.

(33)   Saura, J.; Luque, J. M.; Cesura, A. M.; Prada, M. Da; Chan-Palay, V.; Huber, G.; Löffler, J.; Richards, J. G. Increased Monoamine Oxidase B activity in plaque-associated astrocytes of Alzheimer brains revealed by quantitative enzyme radioautography. *Neuroscience* **1994**, *62* (1), 15–30.

(34)   Tzvetkov, N. T.; Stammler, H. G.; Georgieva, M. G.; Russo, D.; Faraone, I.; Balacheva, A. A.; Hristova, S.; Atanasov, A. G.; Milella, L.; Antonov, L.; et al. Carboxamides vs. methanimines: crystal structures, binding interactions, photophysical studies, and biological evaluation of (Indazole-5-yl)methanimines as Monoamine Oxidase B and Acetylcholinesterase inhibitors. *Eur. J. Med. Chem.* **2019**, *179*, 404–422.

(35)   Kalinowska-Tłuścik, J.; Staroń, J.; Krawczuk, A.; Mordalski, S.; Warszycki, D.; Satała, G.; Hogendorf, A. S.; Bojarski, A. J. The effect of the intramolecular C–H···O interactions on the conformational preferences of bis-arylsulfones – 5-HT$_6$ receptor antagonists and beyond. *RSC Adv.* **2018**, *8* (33), 18672–18681.

(36)   Allen, W. J.; Bevan, D. R. Steered molecular dynamics simulations reveal important mechanisms in reversible Monoamine Oxidase B inhibition. *Biochemistry* **2011**, *50* (29), 6441–6454.

(37) Binda, C.; Hubálek, F.; Li, M.; Herzig, Y.; Sterling, J.; Edmondson, D. E.; Mattevi, A. Crystal structures of Monoamine Oxidase B in complex with four inhibitors of the N-propargylaminoindan Class. *J. Med. Chem.* **2004**, *47* (7), 1767–1774.

(38) Binda, C.; Hubálek, F.; Li, M.; Herzig, Y.; Sterling, J.; Edmondson, D. E.; Mattevi, A. Binding of Rasagiline-related inhibitors to human Monoamine Oxidases: a kinetic and crystallographic analysis. *J. Med. Chem.* **2005**, *48* (26), 8148–8154.

(39) Tandarić, T.; Vianello, R. Computational insight into the mechanism of the irreversible inhibition of Monoamine Oxidase enzymes by the antiparkinsonian propargylamine inhibitors Rasagiline and Selegiline. *ACS Chem. Neurosci.* **2019**, *10* (8), 3532–3542.

(40) Kohen, R.; Fashingbauer, L. A.; Heidmann, D. E.; Guthrie, C. R.; Hamblin, M. W. Cloning of the mouse 5-HT$_6$ serotonin receptor and mutagenesis studies of the third cytoplasmic loop. *Brain Res. Mol. Brain Res.* **2001**, *90* (2), 110–117.

(41) Deraredj Nadim, W.; Chaumont-Dubel, S.; Madouri, F.; Cobret, L.; De Tauzia, M. L.; Zajdel, P.; Benedetti, H.; Marin, P.; Morisset-Lopez, S. Physical interaction between neurofibromin and serotonin 5-HT$_6$ receptor promotes receptor constitutive activity. *Proc. Natl. Acad. Sci. U. S. A.* **2016**, *113* (43), 12310–12315.

(42) Grychowska, K.; Satała, G.; Kos, T.; Partyka, A.; Colacino, E.; Chaumont-Dubel, S.; Bantreil, X.; Wesołowska, A.; Pawłowski, M.; Martinez, J.; et al. Novel 1H-pyrrolo[3,2-c]quinoline based 5-HT$_6$ receptor antagonists with potential application for the treatment of cognitive disorders associated with Alzheimer's Disease. *ACS Chem. Neurosci.* **2016**, *7* (7), 972–983.

(43) Duhr, F.; Déléris, P.; Raynaud, F.; Séveno, M.; Morisset-Lopez, S.; Mannoury la Cour, C.; Millan, M. J.; Bockaert, J.; Marin, P.; Chaumont-Dubel, S. Cdk5 induces constitutive activation of 5-HT$_6$ receptors to promote neurite growth. *Nat. Chem. Biol.* **2014**, *10* (7), 590–597.

(44) Di, L.; Kerns, E. H.; Hong, Y.; Kleintop, T. A.; McConnell, O. J.; Huryn, D. M. Optimization of a higher throughput microsomal stability screening assay for profiling drug discovery candidates. *J. Biomol. Screen.* **2003**, *8* (4), 453–462.

(45) Nicotra, A.; Pierucci, F.; Parvez, H.; Senatori, O. Monoamine oxidase expression during development and aging. *Neurotoxicology* **2004**, *25* (1–2), 155–165.

(46) Chen, J. J.; Swope, D. M.; Dashtipour, K. Comprehensive review of rasagiline, a second-generation monoamine oxidase inhibitor, for the treatment of parkinson's disease. *Clin. Ther.* **2007**, *29* (9), 1825–1849.

(47) Tavari, M.; Malan, S. F.; Joubert, J. Design, synthesis, biological evaluation and docking studies of sulfonyl isatin derivatives as monoamine oxidase and caspase-3 inhibitors. *Med. Chem. Commun.* **2016**, *7* (8), 1628–1639.

(48) Łażewska, D.; Kurczab, R.; Więcek, M.; Kamińska, K.; Satała, G.; Jastrzębska-Więsek, M.; Partyka, A.; Bojarski, A. J.; Wesołowska, A.; Kieć-Kononowicz, K.; et al. The computer-aided discovery of novel family of the 5-HT$_6$ serotonin receptor ligands among derivatives of 4-benzyl-1,3,5-triazine. *Eur. J. Med. Chem.* **2017**, *135*, 117–124.

(49) Grychowska, K.; Kurczab, R.; Śliwa, P.; Satała, G.; Dubiel, K.; Matłoka, M.; Moszczyński-Pętkowski, R.; Pieczykolan, J.; Bojarski, A. J.; Zajdel, P. Pyrroloquinoline scaffold-based 5-HT$_6$R ligands: synthesis, quantum chemical and molecular dynamic studies, and influence of nitrogen atom position in the scaffold on affinity. *Bioorg. Med.*

Chem. **2018**, *26* (12), 3588–3595.

(50)   Glide, Schrodinger, LLC, New York, NY, 2017.

(51)   LigPrep, Schrodinger, LLC, New York, NY, 2017.

(52)   Epik, Schrodinger, LLC, New York, NY, 2017.

(53)   Toledo Warshaviak, D.; Golan, G.; Borrelli, K. W.; Zhu, K.; Kalid, O. Structure-based virtual screening approach for discovery of covalently bound ligands. *J. Chem. Inf. Model.* **2014**, *54* (7), 1941–1950.

(54)   Kurczab, R.; Canale, V.; Satała, G.; Zajdel, P.; Bojarski, A. J. Aminoacid hot spots of halogen bonding: a combined theoretical and experimental case study of the 5-HT$_7$ receptor. *J. Med. Chem.* **2018**, *61* (19), 8717–8733

(55)   Partyka, A.; Kurczab, R.; Canale, V.; Satała, G.; Marciniec, K.; Pasierb, A.; Jastrzębska-Więsek, M.; Pawłowski, M.; Wesołowska, A.; Bojarski, A. J.; et al. The impact of the halogen bonding on D$_2$ and 5-HT$_{1A}$/5-HT$_7$ receptor activity of azinesulfonamides of 4-[(2-ethyl)piperidinyl-1-yl]phenylpiperazines with antipsychotic and antidepressant properties. *Bioorganic Med. Chem.* **2017**, *25* (14), 3638–3648.

(56)   Zajdel, P.; Kos, T.; Marciniec, K.; Satała, G.; Canale, V.; Kamiński, K.; Hołuj, M.; Lenda, T.; Koralewski, R.; Bednarski, M.; et al. Novel multi-target azinesulfonamides of cyclic amine derivatives as potential antipsychotics with pro-social and pro-cognitive effects. *Eur. J. Med. Chem.* **2018**, *145*, 790–804.

(57)   Cheng, Y.; Prusoff, W. H. Relationship between the inhibition constant (K_i) and the concentration of inhibitor which causes 50 per cent inhibition (IC$_{50}$) of an enzymatic reaction. *Biochem. Pharmacol.* **1973**, *22* (23), 3099–3108.

(58)   Stössel, A.; Schlenk, M.; Hinz, S.; Küppers, P.; Heer, J.; Gütschow, M.; Müller, C. E. Dual targeting of adenosine A$_{2A}$ receptors and monoamine oxidase B by 4H-3,1-benzothiazin-4-ones. *J. Med. Chem.* **2013**, *56* (11), 4580–4596.

(59)   Łażewska, D.; Olejarz-Maciej, A.; Reiner, D.; Kaleta, M.; Latacz, G.; Zygmunt, M.; Doroż-Płonka, A.; Karcz, T.; Frank, A.; Stark, H.; et al. Dual target ligands with 4-tert-butylphenoxy scaffold as histamine H$_3$ receptor antagonists and monoamine oxidase B inhibitors. *Int. J. Mol. Sci.* **2020**, *21* (10), 3411–3431.

(60)   Jiang, L. I.; Collins, J.; Davis, R.; Lin, K. M.; DeCamp, D.; Roach, T.; Hsueh, R.; Rebres, R. A.; Ross, E. M.; Taussig, R.; et al. Use of a CAMP BRET sensor to characterize a novel regulation of cAMP by the sphingosine 1-phosphate/G13 pathway. *J. Biol. Chem.* **2007**, *282* (14), 10576–10584.

(61)   Singh, J. K.; Solanki A, S. V. Comparative *in vitro* intrinsic clearance of imipramine in multiple species liver microsomes: human, rat, mouse and dog. *J Drug Metab Toxicol* **2012**, *3*, 126.

(62)   Sumantran, V. N. Cellular Chemosensitivity Assays: An Overview. *Methods Mol. Biol.* **2011**, *731*, 219–236.

(63)   Ennaceur, A.; Delacour, J. A new one-trial test for neurobiological studies of memory in rats. 1: Behavioral data. *Behav. Brain Res.* **1988**, *31* (1), 47–59.

(64)   Popik, P.; Holuj, M.; Nikiforuk, A.; Kos, T.; Trullas, R.; Skolnick, P. 1-Aminocyclopropanecarboxylic acid (ACPC) produces procognitive but not antipsychotic-like effects in rats. *Psychopharmacology (Berl).* **2015**, *232* (6), 1025–1038.